

**Chitosan +
P-407 +
ATO**

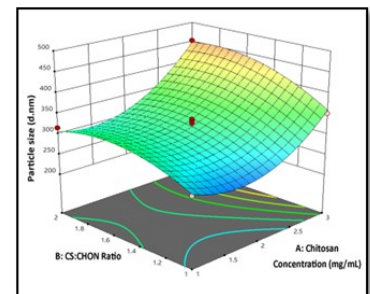
**Add CHON
dropwise into
chitosan solution**



**Stirred at 1000
rpm for 2 hr**



**ATO loaded
PECN**



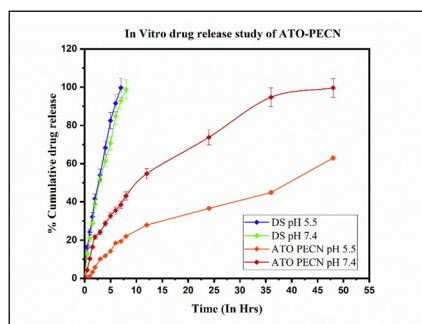
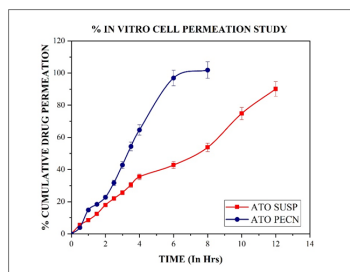
**Optimization of by
BBD**

**Evaluation of
ATO loaded
PECN**

Chapter-7

Formulation development of ATO loaded PECN

**Stability
study**



7.1. Introduction:

Polyelectrolyte complex nanoparticles are three-dimensional networks produced by non-covalent bonding (namely electrostatic, hydrogen, and/or hydrophobic interactions) between polyions with opposing charges, such as polymer-polymer, drug-polymer, and polymer-polymer-drug-polymer [1-4]. Biomimetic nanoparticles have attracted the attention of researchers in recent years as a potential technique for safe drug delivery via skin [5].

7.2. Preparation of ATO loaded PECN:

The ATO loaded PECN were prepared by ionic gelation method or self-assemble complexation method with some modification [6, 7]. The solution of chitosan was prepared in 1 % acetic acid and its pH was adjusted upto 5 with 1M NaOH. Poloxamer 407 was added followed by ATO into chitosan solution and stirred for 15 min. The chondroitin sulfate solution was then added dropwise into the chitosan solution with continuous stirring at 1000 RPM for 2 hrs at 25°C. The resulting nanoparticulate dispersion was centrifuged at 20000 rpm for 20 min (3 cycles) at 20°C, the supernatant was separated and NPs pellet was resuspended in purified water.

7.3. Selection of polyelectrolytes:

In this work, we tried different anionic and cationic polyelectrolytes for preparation of polyelectrolyte complex nanoparticles. Chitosan were tried as cationic polyelectrolytes, while dextran sulfate, hyaluronic acid, pectin, alginate and chondroitin sulfate were tried as anionic polyelectrolytes for development of PECN. The selection of anionic and cationic polyelectrolytes was done based on high entrapment efficiency with minimum particle size.

7.4. Optimization:

After selection of polyelectrolytes, next step was to identify the process and formulation variables that could have a significant effect on the % entrapment efficiency and particle size. The different variables for preliminary include speed of stirring, stirring time, rate of addition, pH of chitosan solution, chitosan concentration, chitosan:chondroitin sulfate ratio and concentration of surfactant. Among these, Chitosan concentration,

chitosan:chondroitin sulfate ratio and pH of chitosan solution showed significant effect on particle size and % EE and were found to be critical variables. Hence, these parameters were further optimized by Box-Behnken design (surface response methodology).

7.5. Screening and optimization of process and formulation parameters:

The process and formulation variables were optimized by one factor at a time (OFAT) approach based on the minimum particle size and maximum entrapment efficiency. The various variables studied for optimization are as follows (table- 7.1):

Table- 7.1. Process and formulation variables studied for ATO loaded PECN formulation development

| | Variables | Screened values/levels | |
|------------------------------|------------------------------------|---|----------------|
| Process variables | Rate of addition (mL/min) | 0.5 | Flash addition |
| | Stirring speed (rpm) | 500 | 2000 |
| | Stirring time (Hr) | 1 | 4 |
| Formulation variables | Surfactant | Tween 80, Brij 58, Poloxamer 188, Poloxamer 407, PVA. | |
| | Surfactant concentration | 0.25 | 1.50 |
| | Chitosan concentration | 1 | 6 |
| | Chitosan:chondroitin sulfate ratio | 0.5:1 | 6:1 |
| | pH of chitosan solution | 3 | 7 |

7.6. Experimental design:

The three level three factor Box-Behnken design (BBD) was used to optimise the ATO loaded PECN and create a polynomial model for the optimization process. BBD is a response surface methodology including various statistical and mathematical methods suitable for the study of difficulties related to the method and experimental errors. It helps to optimise the response that is impacted by many formulation and process-related parameters. The formulation was optimized in order to obtain minimum particle size and maximum entrapment efficiency. The experimental design and their statistical analysis were made by DesignExpert Software (version 13, Sate-Ease Inc. Minneapolis, MN, USA). Total 16 experimental runs were obtained from design, from that, 13 batches

represent mid-point of each edge of multidimensional cube and the residual three runs are replicates of the cube's centre points. Three independent factors were selected viz. Chitosan concentration, chitosan:chondroitin sulfate ratio and pH of chitosan solution. The particle size and entrapment efficiency were selected as dependent variables. Table- 7.2 shows the independent and dependent variables with their levels and goals respectively.

Table- 7.2. Variables investigated in ATO loaded PECN using BBD.

| Variables | Levels | |
|--|---------|------------|
| | Low | High |
| Chitosan concentration (mg/ml) | 1 | 3 |
| CS/CHON ratio | 1:1 | 2:1 |
| pH | 5 | 7 |
| Responses | Goal | Importance |
| Particle Size (d. nm) | Minimum | +++ |
| Entrapment Efficiency (%) | Maximum | +++ |

The check point batch obtained from the design was prepared to validate and confirm batch-to-batch variability.

7.7. Physicochemical characterization of ATO loaded PECN:

a. Particle size, polydispersity index and Zeta potential:

The Z-average particle size, polydispersity index and zeta potential of optimized PEC nanoparticles was characterized by dynamic light scattering (DLS) method using Zetasizer nano ZS-90 (Malvern Instruments, Malvern, UK). The samples were analyzed in triplicates and results represented in average value with standard deviation [8].

b. Entrapment efficiency and loading capacity (%):

The prepared nanoparticles were centrifuged for 20 min at 20000 rpm at 20°C (3 cycles). The supernatant was analyzed by UV visible spectroscopy at 244 nm. The entrapment efficiency (%) was calculated by following formula [7]:

$$\text{Entrapment efficiency (\%)} = \frac{\text{Total ATO added} - \text{Unentrapped ATO}}{\text{Total ATO added}} \times 100$$

..... equation- 7.1.

The loading capacity (%) of formulation was calculated as follows:

$$\text{Loading Capacity} = \frac{\text{Total ATO added} - \text{Unentrapped ATO}}{\text{Total solid content}} \times 100$$

..... equation- 7.2.

c. Morphological analysis:

The surface morphology of ATO loaded PECN was analyzed by transmission electron microscope (TEM, Philips Tecnai 20). The samples stained with phosphotungstic acid solution were put on copper grid, which was coated with carbon and dried at room temperature. TEM was operated at 200 kV to take images of nanoparticles [7].

d. FTIR analysis:

FTIR spectra of samples were obtained using an FTIR spectrophotometer (84000S, Shimadzu, Japan). The samples were mixed with dry KBr (1:100 ratio) and then compressed into discs under 600 to 1000 bar. Drug and optimized formulation were analyzed by FTIR over a range of 4000 to 400 cm^{-1} wavenumber in an inert atmosphere [2, 9].

e. Differential scanning calorimetry (DSC) study:

Differential Scanning Calorimetry analysis was carried out with Shimadzu DSC-60 (Japan). The samples [(a) Drug (ATO), (b) ATO loaded PECN] were placed in aluminium pans and sealed. Thermograms were obtained by heating the samples from 20 to 300°C with a scan rate of 10°C/min with nitrogen supplied at 30 mL/min [10].

f. XRD study:

The X-ray diffraction analysis was analyzed to check the physical state of different components of the optimized formulation by wide angle X-ray scattering (Philips, PW 1710) with a copper anode using Sc as a detector. It was conducted at room temperature and absolute intensity was observed in the range of 10-50 versus 2θ [11, 12].

7.8. *In vitro* drug release study:

The drug release profile from pure drug and ATO loaded PECN was performed by dialysis bag (MW cut-off of 12k-14k Da) in 50 ml of saline phosphate buffer pH 7.4 as well as pH 5.5 (containing 2% of propylene glycol), under magnetic stirring at 100 rpm at 37°C. The samples were withdrawn from diffusion medium at predetermined time interval upto 48 hrs and replaced with same amount of freshly prepared diffusion medium to maintain sink conditions. The withdrawn samples were filtered through 0.45 μm syringe filter and analyzed by UV Visible spectrophotometer at 244 nm.

To describe the release profile, the data was fitted to various exponential equations, including the Zero order, First order, Higuchi, and Korsmeyer-Peppas model [11].

7.9. *Ex vivo* skin permeation study:

Rat skin was mounted on the Franz diffusion cell in such a way that stratum corneum faced the donor receptor and dermis side faced the receptor compartment. The receptor compartment was filled with phosphate buffer 7.4 containing 2% of propylene glycol at $32 \pm 0.5^\circ\text{C}$ under constant magnetic stirring at 100 rpm. The formulations were placed in donor compartment and samples were withdrawn from receptor medium at predetermined time intervals and replaced with freshly prepared medium. The withdrawn samples were filtered through 0.45 μm syringe filter and analyzed by spectrophotometrically [13].

The data was plotted as % cumulative drug permeated through skin as a function of time [14]. The procedure for drug remained on skin and drug retained in the skin was same as described in chapter-5 (section- 5.8.4).

7.10. *In vitro* cell line study:**Cell culture:**

Skin fibroblast cells (3T3) and keratinocytes were purchased from NCCS, Pune, India and grown in T-25 cell culture flask incubated in CO₂ incubator in 5% CO₂ and 100% humidity at 37°C. The culture growth media containing DMEM (high glucose), 10% of foetal bovine serum and 1% of antibiotic solution [15, 16].

1. Cytotoxicity assessment by MTT assay:

The skin fibroblast cells-3T3 [17] (7500 cells/well) were seeded in 96-well plates filled with 200 µl of culture growth medium. After 24 hrs, the cells were washed with sterile phosphate buffer 7.4 and replaced with fresh growth medium. Then cells were treated for 12 and 24 hrs with pure drug, placebo formulation and drug loaded PECN in triplicates. Untreated cells were used as negative control. After completion of treatment period, the cells were washed with fresh medium at least three times and MTT reagent (1mg/ml in PBS) was added to each well. After 2-3 hrs, formed formazan crystals were dissolved in 100 µl of dimethyl sulfoxide and their concentration was spectrophotometrically quantified at 570 nm with a microplate reader (680 XR, Bio-rad Laboratories, USA). The results were represented as % of cell viability in comparison with non-treated cells [18, 19].

2. *In vitro* cell permeability study:

In vitro cell permeability study was performed across fibroblasts and keratinocytes monolayer (apical to basolateral). Transwell® inserts of 12 mm diameter, 0.4 µm pore size (Corning, USA) with surface area of 1.12 cm² were used. According to standard protocol for permeability study, fibroblast cells were cultivated on filter support at a density of 4*10⁵ cells per well. The cells were maintained by changing media every alternate day for 21 days. The integrity of the monolayers was checked by monitoring the trans-epithelial resistance measurement using Millicell® ERS meter (Millipore, Bedford, Massachusetts, USA). After incubation, transepithelial permeation from AP to BL was carried out by placing pure drug and their formulations equivalent to 300 µg prepared in growth medium on the AP side, and 2.5 mL of DMEM on the BL side. Samples (200 µL) were withdrawn from BL compartments at predetermined time

interval over 12 hrs. Withdrawn samples were stored at -20 °C until analysis by HPLC (as described in *in vitro* drug release study). The apparent permeability coefficient (P_{app} in cm/s) from apical-to-basolateral was calculated as follows:

$$P_{app} = \frac{\text{Flux}}{\text{Initial concentration}} \quad \dots \dots \dots \text{equation} - 7.3.$$

Where, P_{app} is the apparent permeability co-efficient (cm/s) [20-22].

7.11. Stability study:

The storage stability of drug loaded PECN dispersion was carried out at 2-8 °C, 25 ± 2°C/60 ± 5% RH and 40 ± 2°C/75 ± 5% RH in air tight container for 90 days. Samples were monitored by analysing for average particle size and % assay at interval of 15 days [23, 24].

7.12. Results and discussion:

ATO loaded PECN: Formulation development

The current study covers the fabrication and evaluation of ATO-loaded PECN, as well as the determination of many crucial factors that determine particle size and % EE. After the identification and selection of essential variables, preliminary study was performed to determine optimal operating ranges, which were then used to optimise each of the parameters using surface response methodology.

7.13. Preliminary screening for ATO loaded PECN:

7.13.1. Selection of polyelectrolytes:

An important set of criteria for development of PECN is selection of cationic and anionic polyelectrolytes. Among the several polyelectrolytes, the prepared PECN of Chitosan (used as cationic polyelectrolyte) and chondroitin sulfate (used as anionic polyelectrolyte) showed minimum particle size and high entrapment efficiency (shown in table- 7.3). Hence, chitosan and chondroitin sulfate selected as cationic and anionic polyelectrolyte respectively for preparation of PECN.

Table- 7.3. Selection of polyelectrolytes

| Selection of polyelectrolytes | | | |
|-------------------------------|---------------------|-------------------------|------------------------------|
| Polyelectrolytes | | Results | |
| Cationic | Anionic | Particle Size (d.nm) | Entrapment efficiency (%) |
| | Dextran sulfate | 355.9 ± 5.84 | 60.84 ± 1.33 |
| | Hyaluronic acid | 386.7 ± 7.41 | 63.58 ± 2.71 |
| Chitosan | Chondroitin sulfate | 251.3 ± 4.12 | 74.66 ± 1.68 |
| | Sodium alginate | 418.8 ± 4.69 | 55.74 ± 3.84 |
| | Pectin | 401.6 ± 8.94 | 59.48 ± 2.18 |

(n=3, ± S.D.)

7.13.2. Risk analysis and mitigation:

After the selection of polyelectrolytes, a risk analysis was conducted for the formulation of ATO loaded PECN. Risk analysis is nothing but the determination of important factors, the slight change in which can result in decline in product quality. The FishBone diagram (Figure- 7.1) was constructed on the basis of literature review to identify formulation and process variables that might alter the quality of PECN. The quality target or Critical Quality Attributes (CQA) for ATO loaded PECN was high entrapment efficiency with small particle size, as these factors are connected to the therapeutic efficacy of the prepared PECN. During the preliminary tests, the variables with a low or medium influence on the PECN were optimised using the One Variable At a Time (OVAT) technique, whilst the high-risk factors (shown in table-7.4) were optimised using the Box-Behnken design (BBD). Only process and formulation factors were examined for risk analysis in this case, whereas drug substance properties were assumed to be constant because the drug utilised was of the same lot number throughout the study.

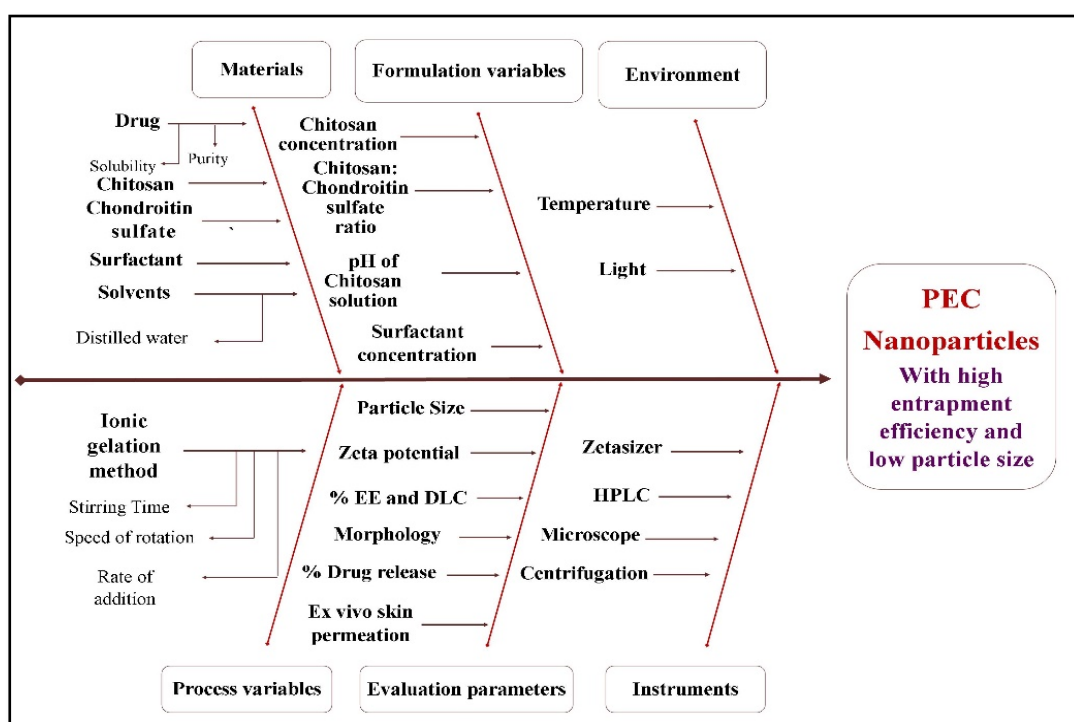


Figure- 7.1. FishBone diagram for selection of variables for development of PECN

Table- 7.4. Risk analysis to identify critical parameters for formulation of ATO loaded PECN

| Critical Quality Attributes (CQA) | Process variables | | | Formulation Variables | | | |
|-----------------------------------|-------------------|----------------|------------------|--------------------------------|-------------------------------------|-------------------------|------------------------------|
| | Stirring time | Stirring speed | Rate of addition | Chitosan concentration (mg/dL) | Chitosan: chondroitin sulfate ratio | pH of chitosan solution | Surfactant concentration (%) |
| Particle Size (d.nm) | L | M | M | H | H | H | M |
| Entrapment efficiency (%) | L | M | L | H | H | H | M |

7.13.3. Screening and optimization of process parameters for preparation of PECN:

The process parameters for preparation of ATO loaded PECN such as such as rate of addition, speed of rotation and stirring time were screened and optimized (shown in table- 7.5) as follows:

a. Selection of rate of addition:

The inadequate rate of addition results in formation of bigger particles. Flash addition showed the aggregation of particles. The 1.0 mL/min rate of addition showed smaller particle size and maximum entrapment efficiency rather than 0.5 mL/min and 2.0 mL/min. This might be explained by the higher concentration of CHON at the interface between the two solutions when adding at higher rates. As a consequence, there were more inter and intra cross-linkages, which resulted in bigger particles [25]. Based on maximum entrapment efficiency and minimum particle size, 1.0 mL/min of rate of addition selected as optimum for further development.

b. Selection of speed of rotation:

The particle size of PECN decreased with an increase in the speed of rotation from 500 to 1000 rpm. This happens due to an increase in the shear force, which has the effect of accelerating CHON dispersion in the chitosan solution, leading to more inter- and intra-cross-linkages in chitosan [25-27]. Beyond an increase in stirring speed up to 1500 rpm, there is an increase in particle size and a lowering of EE due to the fact that at higher stirring speeds, particles may aggregate due to the destruction of the repulsive force between the particles [7, 12, 28]. On the basis of the results, 1000 rpm was selected as the speed of rotation for further development.

c. Selection of stirring time:

The stirring time mainly effects on the quality of prepared nanoparticles. The results showed that an increase in stirring time results in a decrease in particle size and an increase in entrapment efficiency. The stirring time of 2 hours was sufficient to prepare nanoparticles with a minimum PS and high EE due to the fact that it provided sufficient time to take orientation and prolong the exposure of chitosan to chondroitin

sulfate for the formation of PECN [29]. On the basis of the results, 2 hours was selected as the optimum stirring time for further development.

Table- 7.5. Effect of process parameters on preparation of ATO loaded PECN

| Selection of rate of addition (mL/min) | | |
|---|---------------------|--------------|
| Selection of rate of addition (mL/min) | Observations | |
| | PS (d.nm) | % EE |
| Flash addition | 562.6 ± 5.47 | 61.85 ± 1.65 |
| 0.5 | 400.0 ± 6.41 | 63.15 ± 2.95 |
| 1.0 | 258.8 ± 2.36 | 75.40 ± 2.08 |
| 2.0 | 344.9 ± 5.25 | 68.53 ± 2.74 |
| Selection of speed of rotation (RPM) | | |
| Selection of speed of rotation (RPM) | Observations | |
| | PS (d.nm) | % EE |
| 500 | 357.7 ± 8.74 | 64.08 ± 2.66 |
| 1000 | 243.7 ± 4.15 | 78.18 ± 2.14 |
| 1500 | 495.8 ± 5.17 | 58.15 ± 1.67 |
| 2000 | 521.1 ± 10.12 | 55.27 ± 2.31 |
| Selection of stirring time (Hrs) | | |
| Selection of stirring time (Hrs) | Observations | |
| | PS (d.nm) | % EE |
| 0.5 | 375.4 ± 12.18 | 64.36 ± 2.46 |
| 1.0 | 337.9 ± 8.14 | 68.69 ± 2.54 |
| 2.0 | 238.4 ± 5.73 | 76.17 ± 1.76 |
| 3.0 | 232.5 ± 7.36 | 74.36 ± 1.58 |

(n=3, ± S.D.)

7.13.4. Screening and optimization of formulation parameters for PECN preparation:

The screening and optimization of formulation parameters such as chitosan concentration, chitosan:chondroitin sulfate ratio, pH of the chitosan solution, surfactant, and concentration of surfactant is shown in table- 7.6:

Table- 7.6. Effect of formulation parameters on preparation of ATO loaded PECN

| Screening of surfactant | | |
|---|---------------------|--------------|
| Surfactant | Observations | |
| | PS (d.nm) | % EE |
| Tween 80 | 404.6 ± 8.24 | 64.56 ± 1.28 |
| Brij 58 | 425.1 ± 5.62 | 67.96 ± 1.69 |
| Poloxamer 188 | 322.3 ± 3.98 | 69.06 ± 1.37 |
| Poloxamer 407 | 253.4 ± 2.84 | 74.86 ± 2.63 |
| PVA | 300.9 ± 4.95 | 66.16 ± 1.05 |
| Screening of concentration of surfactant | | |
| Concentration of surfactant (%) | Observations | |
| | PS (d.nm) | % EE |
| 0.25 | 547.4 ± 8.47 | 65.16 ± 2.63 |
| 0.50 | 474.3 ± 7.77 | 66.06 ± 2.36 |
| 0.75 | 368.3 ± 6.45 | 69.46 ± 3.21 |
| 1.00 | 253.4 ± 5.14 | 74.06 ± 2.02 |
| 1.25 | 244.6 ± 5.15 | 71.21 ± 1.58 |
| 1.50 | 230.5 ± 6.32 | 75.11 ± 3.47 |
| Chitosan concentration (mg/mL) | | |
| Chitosan concentration (mg/mL) | Observations | |
| | PS (d.nm) | % EE |
| 1 | 230.8 ± 2.15 | 54.15 ± 1.89 |
| 2 | 282.7 ± 4.52 | 77.81 ± 2.10 |
| 3 | 316.1 ± 6.33 | 70.11 ± 2.36 |
| 4 | 348.3 ± 5.21 | 66.25 ± 2.51 |
| 6 | 343.9 ± 4.58 | 67.61 ± 3.25 |

| Chitosan:chondroitin sulfate ratio | | |
|---|---------------------|--------------|
| Chitosan:chondroitin sulfate ratio | Observations | |
| | PS (d.nm) | % EE |
| 0.5:1 | 342.1 ± 8.22 | 59.02 ± 2.56 |
| 1:1 | 250.3 ± 5.21 | 78.13 ± 2.41 |
| 1.5:1 | 380.8 ± 6.33 | 72.05 ± 1.62 |
| 2:1 | 403.4 ± 4.25 | 64.03 ± 1.57 |
| 3:1 | 522.6 ± 5.84 | 66.78 ± 2.96 |
| pH of chitosan solution | | |
| pH of chitosan solution | Observations | |
| | PS (d.nm) | % EE |
| 3 | 502.3 ± 8.25 | 54.10 ± 3.84 |
| 4 | 444.5 ± 6.61 | 68.65 ± 2.51 |
| 5 | 246.2 ± 5.14 | 78.33 ± 2.08 |
| 6 | 341.4 ± 5.12 | 70.13 ± 2.83 |
| 7 | 393.0 ± 4.87 | 54.08 ± 2.43 |

(n=3, ± S.D.)

a. Screening of surfactant:

There were different surfactants screened, among which poloxamer 407 was selected for further development due to its lower PS and higher EE than other surfactants (shown in table- 7.6).

b. Screening of surfactant concentration:

The surfactant concentration was varied from 0.25 %w/v to 1.5 % w/v, and from the results, it was found that an increase in surfactant concentration leads to a decrease in particle size with an increase in EE. Particle size was reduced by increasing the concentration of surfactant because it works by decreasing interfacial tension which can prevent the coalescence or aggregation of particles [11]. But 0.25% %w/v poloxamer 407 was insufficient to stabilize the nanoparticles, resulting in the

formation of larger nanoparticles. Beyond 1.0 %w/v surfactant concentration, no remarkable difference was found in EE or PS. Overall, no significant difference was found in the entrapment efficiency with an increase in the concentration of surfactant. On the basis of results, 1.0 %w/v of poloxamer 407 was selected as optimum surfactant concentration for further development.

c. Screening of chitosan concentration:

The results of preliminary screening of chitosan concentration showed that increase in the concentration of chitosan increases particle size with increase in entrapment efficiency upto certain level and further increase in concentration of chitosan decreases entrapment efficiency with increase in particle size. Beyond 3 mg/mL, lowered EE may be caused by the fact that when chitosan concentration increased, CHON remains constant and is unable to interact with all available chitosan [3, 5]. Beyond 4 mg/mL of chitosan concentration, no remarkable difference was found in EE and particle size. Hence, the range of 1 mg/mL to 3 mg/mL was selected for further optimization.

d. Screening of chitosan:chondroitin sulfate ratio:

The optimum CS:CHON ratio is required for formation of stable polyelectrolyte complex nanoparticles. Aggregation of nanoparticles occurs when the ratio goes below or above this ratio [5]. The results showed that the increase in CS:CHON ratio increases particle size and decreases EE up to a certain level; beyond that, the increase in ratio decreases EE with an increase in PS. This observation might be attributable to the fact that decreasing the ratio improved the effect of CHON on the synthesis medium, allowing more NH_3^+ groups of CS to be neutralized by the CHON negative charge and eventually decreasing the particle size [5, 10]. The decrease in the CS:CHON ratio resulted in an increase in EE due to the formation of tightly crosslinked PECN, which prevents the leakage of drug from nanoparticles. There was no remarkable difference found in PS and EE between 2:1 and 3:1 of the CS:CHON ratio. The increase in PS and decrease in EE observed at a 0.5:1 CS:CHON ratio might be due to the increased concentration of chondroitin sulfate as compared to chitosan, which leads to an increase in intermolecular attraction due to the presence of excess $-\text{SO}_3^-$ in the solution, resulting in an increase in particle

size. Hence, on the basis of the results, a 1:1 to 2:1 ratio of CS:CHON was selected for further optimization.

e. pH of chitosan solution:

The pH of the chitosan solution plays an important role in the development of PECN. The PEC nanoparticles form between oppositely charged polymers, which depend on the ionic strength of the polymers. If two polymers interact, a successful formation of PEC nanoparticles can only take place at a pH that is within the pKa values of the two polymers, allowing for increased ionic interaction and ionization of the two polymers [5, 30]. The change in pH of chitosan solution directly effects on particle size as well as EE. The results showed that increase in pH of chitosan solution leads to decrease in particle size with increase in EE upto pH 5. But beyond that, increase in pH results in increase in particle size with decrease in EE might be due presence of fewer -NH_3^+ density available for interaction with -SO_3^- at higher pH or pH nearer to pKa value of chitosan . At lower pH of the chitosan solution, i.e., 3 and 4, larger size nanoparticles were formed and settled down within 48 hours. On the basis of result, a pH range of 5 to 7 for the chitosan solution was chosen for further optimization.

Using a design of experiment technique, the high-risk parameters were optimised while keeping other process and formulation variables constant.

7.14. Experimental design and analysis of results:

The ATO loaded PEC nanoparticles were prepared and optimized by BBD. All 16 experimental runs with their responses are shown in table- 7.7. The quadratic model was found to be best fit for all responses and the predicted and observed values were found to be very close to each other. The polynomial equations were generated which explained the individual main effects and interaction effects of independent factors on each dependent variables by Design-Expert V.13.0 version software (Stat-Ease, Inc., USA).

Table – 7.7. Experimental runs of ATO loaded PECN by BBD

| Run | Factor 1 | Factor 2 | Factor 3 | Response 1 | Response 2 |
|-----|----------------------------------|-------------------|-----------------------------|----------------------|--------------|
| | A : Chitosan Concentration mg/ml | B : CS:CHON Ratio | C : pH of chitosan solution | Particle Size (d.nm) | EE (%) |
| 1 | 1 | 1.5:1 | 5 | 252.2 ± 5.99 | 50.27 ± 0.66 |
| 2 | 2 | 1:1 | 5 | 214.3 ± 4.65 | 80.79 ± 1.55 |
| 3 | 2 | 1:1 | 7 | 296.1 ± 7.75 | 66.35 ± 1.84 |
| 4 | 2 | 1.5:1 | 6 | 302.2 ± 4.34 | 64.65 ± 2.51 |
| 5 | 3 | 1.5:1 | 7 | 484.6 ± 9.91 | 58.20 ± 2.36 |
| 6 | 1 | 2:1 | 6 | 316.2 ± 4.94 | 47.07 ± 1.75 |
| 7 | 2 | 2:1 | 7 | 340.2 ± 3.92 | 56.98 ± 1.29 |
| 8 | 1 | 1:1 | 6 | 268.8 ± 7.01 | 53.37 ± 1.06 |
| 9 | 2 | 1.5:1 | 6 | 328.2 ± 3.52 | 61.18 ± 0.53 |
| 10 | 2 | 1.5:1 | 6 | 310.9 ± 5.02 | 60.40 ± 1.05 |
| 11 | 3 | 1.5:1 | 5 | 385.1 ± 2.46 | 73.70 ± 1.01 |
| 12 | 2 | 2:1 | 5 | 267.9 ± 3.75 | 74.25 ± 0.66 |
| 13 | 3 | 2:1 | 6 | 452.8 ± 1.21 | 69.22 ± 1.09 |
| 14 | 3 | 1:1 | 6 | 351.4 ± 4.42 | 67.15 ± 2.26 |
| 15 | 1 | 1.5:1 | 7 | 379.9 ± 3.43 | 40.29 ± 1.82 |
| 16 | 2 | 1.5:1 | 6 | 337.3 ± 3.90 | 63.85 ± 2.10 |

(n=3, ± S.D.)

All the batches were prepared in triplicate and evaluated for particle size and entrapment efficiency. The effect of independent variables on response is discussed below:

7.14.1. Effects of independent variables on particle size:

The values of particle size varied from 214.3 to 484.6 d.nm throughout all 16 runs due to variation in independent factor combinations. From the statistical analysis, we can observe that R^2 value for actual Vs predicted values for particle size was 0.7595 which is good correlation.

ANOVA results of model:

Summary of the ANOVA results of different models for particle size is shown in table-7.8 which depicts model p-value with adjusted and predicted R² values.

Table- 7.8. Summary of ANOVA results of different models for particle size

| Source | Sequential p-value | Lack of Fit p-value | Adjusted R ² | Predicted R ² | |
|-----------|--------------------|---------------------|-------------------------|--------------------------|------------------|
| Linear | 0.0020 | 0.0445 | 0.6184 | 0.3703 | |
| 2FI | 0.9395 | 0.0275 | 0.5124 | -0.4608 | |
| Quadratic | 0.0012 | 0.4046 | 0.9396 | 0.7595 | Suggested |
| Cubic | 0.4046 | | 0.9487 | | Aliased |

The polynomial showed lowest p-value ($p < 0.05$) which was considered for model selection. Based on the results obtained from the experiments and criteria, quadratic model was suggested to be best fitted to the observed responses. Other models were not suitable for prediction either due to low R² value or due to high p value as compared to quadratic model. The significant and insignificant terms are classified based on p value, which means those models with p-values less than 0.05 are significant, while others are insignificant [31].

The results of ANOVA (shown in table- 7.9) revealed that the effect of factors was significant and hence the model is significant for the particle size. The Model F-value of 26.94 implies the model is significant. There is only a 0.04% chance that an F-value this large could occur due to noise. P-values less than 0.0500 indicate model terms are significant. In this case A, B, C, A², B² are significant model terms. The **Lack of Fit F-value** of 1.35 implies the Lack of Fit is not significant relative to the pure error. Non-significant lack of fit is good.

Table- 7.9. ANOVA results of quadratic model for particle size

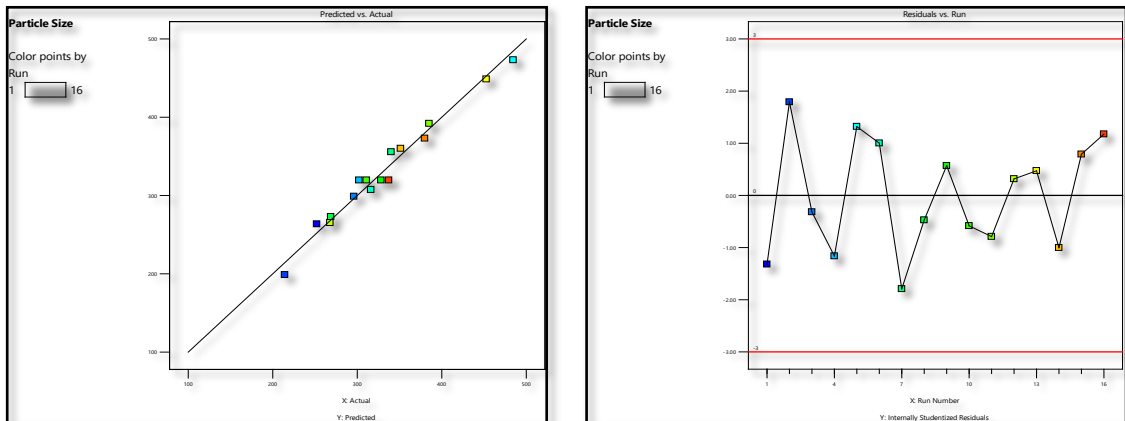
| Source | Sum of Squares | df | Mean Square | F-value | p-value | |
|---------------------------------|----------------|----|-------------|---------|----------|-----------------|
| Model | 72837.57 | 9 | 8093.06 | 26.94 | 0.0004 | Significant |
| A-Chitosan Concentration | 26083.28 | 1 | 26083.28 | 86.83 | < 0.0001 | |
| B-CS:CHON Ratio | 7595.28 | 1 | 7595.28 | 25.28 | 0.0024 | |
| C-pH | 18173.71 | 1 | 18173.71 | 60.50 | 0.0002 | |
| AB | 729.00 | 1 | 729.00 | 2.43 | 0.1703 | |
| AC | 198.81 | 1 | 198.81 | 0.6618 | 0.4470 | |
| BC | 22.56 | 1 | 22.56 | 0.0751 | 0.7932 | |
| A² | 15246.08 | 1 | 15246.08 | 50.75 | 0.0004 | |
| B² | 4647.83 | 1 | 4647.83 | 15.47 | 0.0077 | |
| C² | 141.02 | 1 | 141.02 | 0.4694 | 0.5188 | |
| Residual | 1802.36 | 6 | 300.39 | | | |
| Lack of Fit | 1036.67 | 3 | 345.56 | 1.35 | 0.4046 | Not significant |
| Pure Error | 765.69 | 3 | 255.23 | | | |
| Cor Total | 74639.93 | 15 | | | | |

Table- 7.10. Summary of ANOVA results for particle size

| Parameters | Results | Parameters | Results |
|------------------|---------|--------------------------------|---------|
| Std. Dev. | 17.33 | R² | 0.9759 |
| Mean | 330.51 | Adjusted R² | 0.9396 |
| C.V. % | 5.24 | Predicted R² | 0.7595 |
| | | Adeq Precision | 20.0253 |

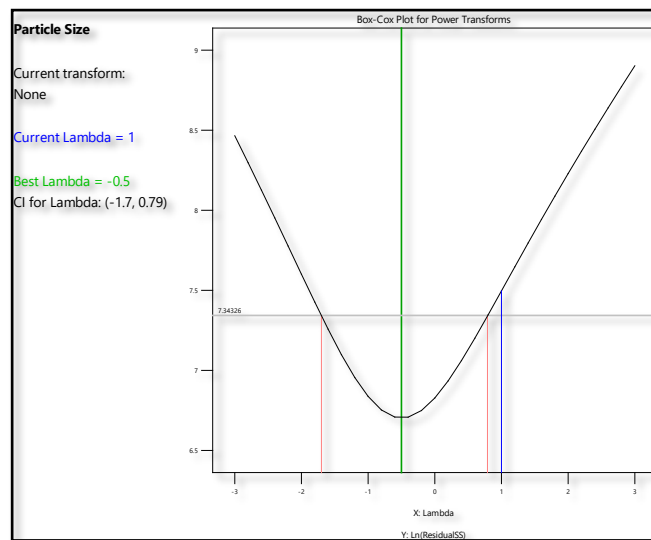
The Predicted R² of 0.7595 is in reasonable agreement with the Adjusted R² of 0.9396; i.e. the difference is less than 0.2 (shown in table- 7.10). The Adeq Precision measures the signal to noise ratio. A ratio greater than 4 is desirable. The ratio of 20.025 indicates an adequate signal. This model can be used to navigate the design space.

Model diagnostic plots:



a. Predicted Vs actual

b. Residual vs run



c. Box-Cox plot for power transforms

Figure- 7.2. Model diagnostic plots for particle size

- a. Predicted Vs actual plot
- b. Residual vs run plot
- c. Box-Cox plot for power transforms

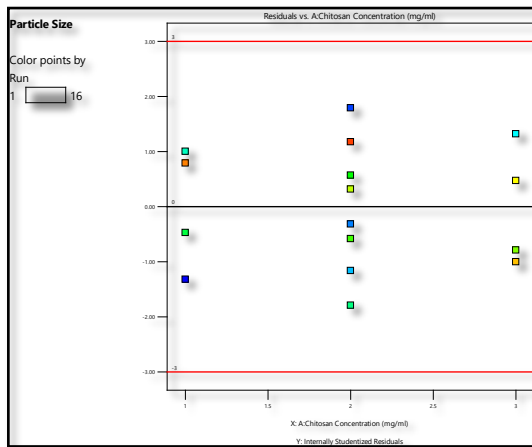
Various diagnostic plots for evaluation of model are shown in figure-7.2.

The **predicted vs. actual plot** (figure- 7.2a) depicts the relationship between observed and actual response values. A strong correlation between the predicted and actual values (data following a straight 45° line) indicates that the model chosen for data analysis is accurate in predicting responses throughout the design matrix. This graphic also helps

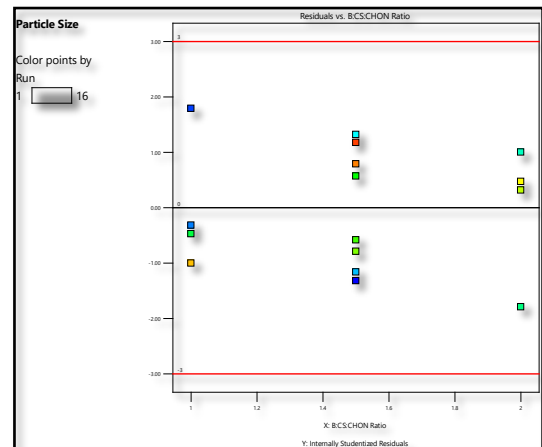
in detecting values that are not easily predicted by the model [32]. The predicted vs actual plot follows a 45° straight line which indicates a close estimation of actual values with predicted values.

A graph of the **residuals vs the order of the experimental runs** (figure-7.2b). The **residual vs run plot** (figure- 7.2b) shows random distribution of residuals in the current analysis indicating that absence of hidden variable.

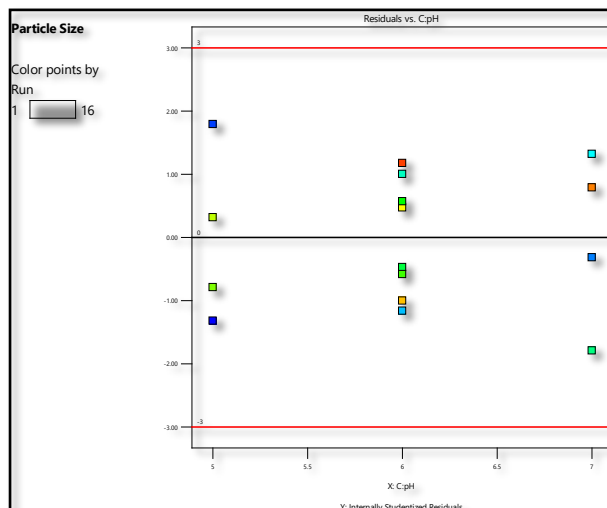
The **Box-Cox plot** (figure- 7.2c) showed that the best λ values (0.5), which lie nearer to the current λ value of 1 and found within 95% CI of it (-1.7 to 0.79), indicated that there was no power transformation required.



a. Residual Vs Chitosan concentration



b. Residual Vs CS:CHON ratio



c. Residual Vs pH of chitosan solution

Figure- 7.3. Residual Vs factor plots

- a. Residual Vs Chitosan concentration
- b. Residual Vs CS:CHON ratio
- c. Residual Vs pH of chitosan solution

Figures-7.3 a–c represents the plot of **residuals vs. selected factors**. The plots for each factor showed a random dispersion throughout the increasing level of factor, demonstrating that the model is effective in accounting for the variation for each variable.

Model plots: Response surface plot (3D plot):

The value of ANOVA gives us idea about the factors having significant effect on particle size which is shown in 3D plots. In this plot, the red area represents the maximum particle size and blue area represents the lowest particle size.

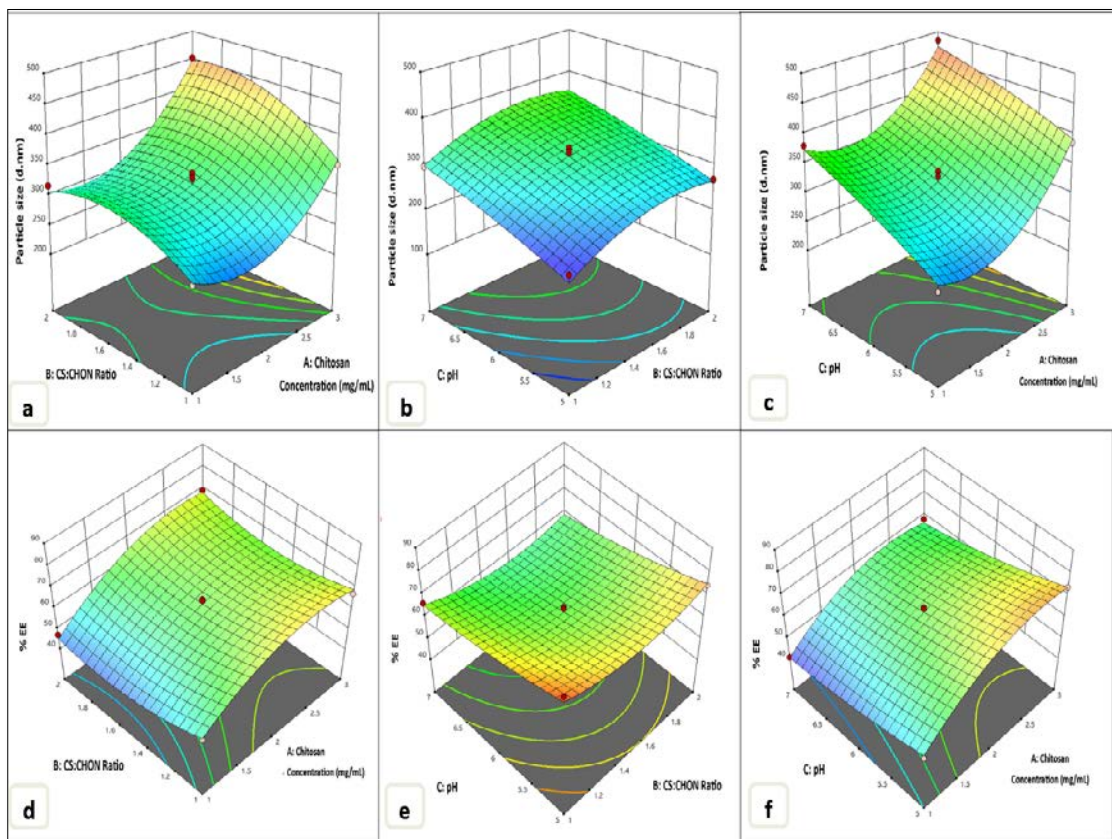


Figure- 7.4. 3D surface plot for showing effects of independent factors on particle size

- a. Chitosan concentration and CH:CHON ratio
- b. Chitosan concentration and pH of chitosan solution
- c. CH:CHON ratio and pH of chitosan solution

- Effects of independent factors on % EE.
- d. Chitosan concentration and CH:CHON ratio
 - e. Chitosan concentration and pH of chitosan solution
 - f. CH:CHON ratio and pH of chitosan solution

The 3D surface plot (figure- 7.4a) revealed that as the concentration of chitosan increased, the particle size of nanoparticles increased. The positive magnitude of factor A also showed the positive response of chitosan concentration on particle size i.e., increase in particle size with increase in concentration of chitosan. At low chitosan solution concentration, the electrostatic forces between sulfate, and carboxylate anions of CHON and the protonated amine groups of chitosan predominated over the attractive forces created by the intermolecular hydrogen bonding between chitosan molecules which could explain the above trend. At higher chitosan concentrations, there is a higher density of protonated amine groups available, causing greater repulsion among them and leading to an increase in particle size [10].

From the 3D surface plot (figure- 7.4b), it was concluded that as the CS:CHON ratio increases, the particle size increases. The positive magnitude in the polynomial equation also revealed that the particle size increases with an increase in the CS:CHON ratio due to the fact that more NH_3^+ groups were neutralised by the CHON negative charge, and finally the resistance of the CS molecules was overcome, leading to a reduction in particle size. Excess CS molecules strengthened the intermolecular attraction forces between CS molecules and resisted the electrostatic attraction force between CHON anions and NH_3^+ cations, resulted in the formation of larger size nanoparticles [10, 12].

The 3D surface plot (figure- 7.4c) also showed positive correlation of pH with particle size, that is, increase in particle size with increase in pH of chitosan solution. At $\text{pH} > 5$, there was a fewer amount of NH_3^+ groups available for interaction at pH values closer to the pKa of chitosan i.e., 6.3 and 7.2. Hence, at pH 5 to 6 the particle size is significantly lower as compared to higher pH. In case of PEC nanoparticles, at pH near to 5.0 of chitosan solution, maximum number of ions existed in solution which react with oppositely charge ions and allows the formation of nanoparticles with tight crosslinking and small particle size [2, 10].

Polynomial equation for Particle size:

The polynomial equations were obtained from design for particle size as follows:

Final equation in terms of coded factors:

$$\begin{aligned} \text{Particle Size (d.nm)} &= +319.65 + 57.10 * A + 30.81 * B + 51.41 * C + \\ &13.50 * AB - 7.05 * AC - 2.38 * BC + 61.74 * \\ &A^2 - 34.09 * B^2 - 5.94 * C^2 \end{aligned}$$

..... equation- 7.4.

Reduced equation in terms of coded factors:

$$\begin{aligned} \text{Particle Size (d.nm)} &= +319.65 + 57.10 * A + 30.81 * B + 51.41 * C + \\ &61.74 * A^2 - 34.09 * B^2 \end{aligned}$$

..... equation- 7.5.

7.14.2. Effects of variables on % EE:

The values of entrapment efficiency varied from 40.29 to 80.79% throughout all 16 runs due to variation in independent factor combination.

ANOVA results of model:

Summary of the ANOVA results of different models for % EE is shown in table-7.11 which depicts model p-value with adjusted and predicted R² values. From the statistical analysis, we can observe that R² value for actual Vs predicted values for % EE was 0.7456 which is good correlation.

Table- 7.11. Summary of ANOVA results of different models for % EE

| Source | Sequential p-value | Lack of Fit p-value | Adjusted R ² | Predicted R ² | |
|-----------|--------------------|---------------------|-------------------------|--------------------------|------------------|
| Linear | 0.0015 | 0.0303 | 0.6387 | 0.3972 | |
| 2FI | 0.9101 | 0.0190 | 0.5450 | -0.3901 | |
| Quadratic | 0.0012 | 0.2879 | 0.9438 | 0.7456 | Suggested |
| Cubic | 0.2879 | | 0.9629 | | Aliased |

The polynomial which showed the lowest p values (<0.05) was considered for model selection. On the basis of criteria, the quadratic model was found to be best fitted to the observed responses and chosen for further evaluation.

Table- 7.12. ANOVA results of quadratic model for % EE

| Source | Sum of Squares | df | Mean Square | F-value | p-value | |
|----------------------------------|----------------|----|-------------|---------|----------|-----------------|
| Model | 1657.90 | 9 | 184.21 | 28.97 | 0.0003 | Significant |
| A-Chitosan Concentration | 746.33 | 1 | 746.33 | 117.35 | < 0.0001 | |
| B-CS:CHON Ratio | 50.70 | 1 | 50.70 | 7.97 | 0.0302 | |
| C-pH of chitosan solution | 408.84 | 1 | 408.84 | 64.28 | 0.0002 | |
| AB | 17.51 | 1 | 17.51 | 2.75 | 0.1481 | |
| AC | 7.62 | 1 | 7.62 | 1.20 | 0.3157 | |
| BC | 2.00 | 1 | 2.00 | 0.3148 | 0.5951 | |
| A² | 299.12 | 1 | 299.12 | 47.03 | 0.0005 | |
| B² | 113.64 | 1 | 113.64 | 17.87 | 0.0055 | |
| C² | 12.15 | 1 | 12.15 | 1.91 | 0.2162 | |
| Residual | 38.16 | 6 | 6.36 | | | |
| Lack of Fit | 25.56 | 3 | 8.52 | 2.03 | 0.2879 | Not significant |
| Pure Error | 12.60 | 3 | 4.20 | | | |
| Cor Total | 1696.06 | 15 | | | | |

The ANOVA results for quadratic model for % EE is shown in table- 7.12. The Model F-value of 28.97 implies the model is significant. There is only a 0.03% chance that an F-value this large could occur due to noise. The P-values less than 0.0500 indicate model terms are significant. In this case A, B, C, A², B² are significant model terms. Values greater than 0.1000 indicate the model terms are not significant. If there are many insignificant model terms (not counting those required to support hierarchy),

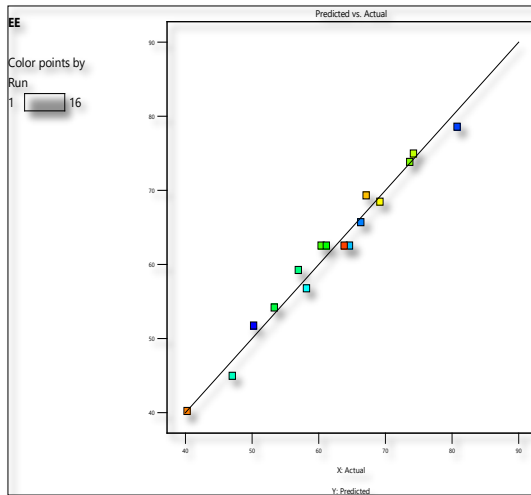
model reduction may improve your model. The Lack of Fit F-value of 2.03 implies the Lack of Fit is not significant relative to the pure error. There is a 28.79% chance that a Lack of Fit F-value this large could occur due to noise. Non-significant lack of fit is good and it want the model to fit.

Table- 7.13. Summary of ANOVA results for % EE

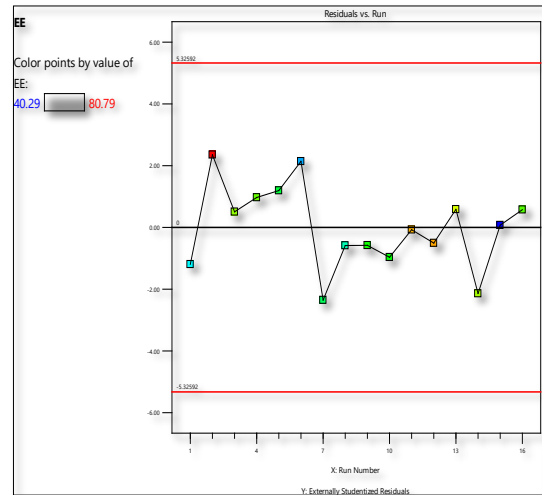
| Parameters | Values | Parameters | Values |
|------------|--------|--------------------------|---------|
| Std. Dev. | 2.52 | R ² | 0.9775 |
| Mean | 61.73 | Adjusted R ² | 0.9438 |
| C.V. % | 4.09 | Predicted R ² | 0.7456 |
| | | Adeq Precision | 19.2424 |

The Predicted R² of 0.7456 is in reasonable agreement with the Adjusted R² of 0.9438; i.e. the difference is less than 0.2 (shown in table- 7.13). The Adeq Precision measures the signal to noise ratio. A ratio greater than 4 is desirable. The ratio of 19.242 indicates an adequate signal. This model can be used to navigate the design space.

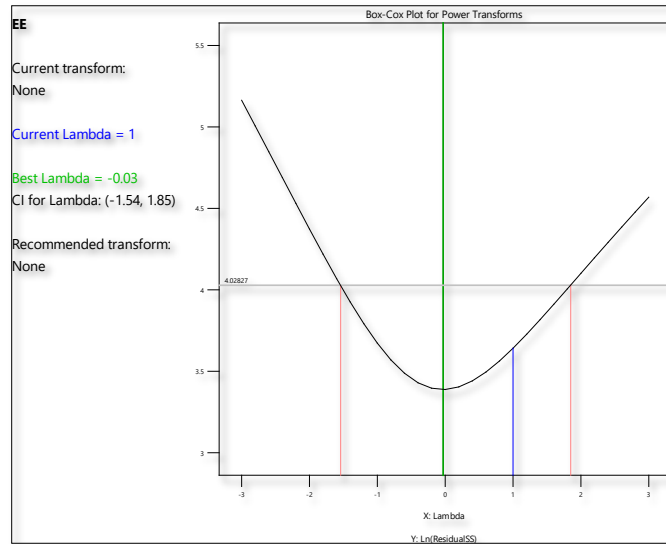
Model diagnostic plots:



a. Predicted Vs actual



b. Residual vs run

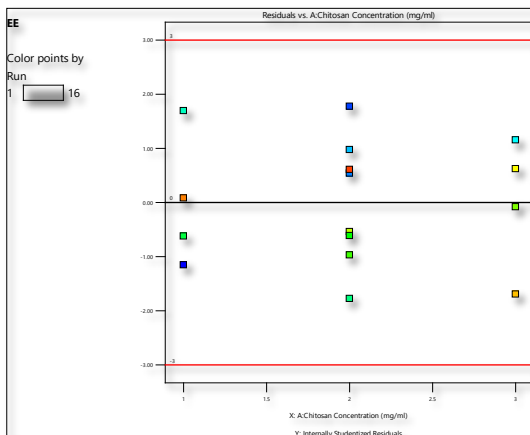


c. Box-Cox plot for power transforms

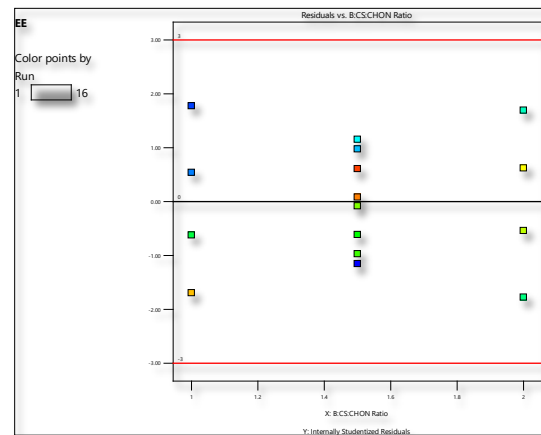
Figure– 7.5. Model diagnostic plots for % EE

- a. Predicted Vs actual plot
- b. Residual vs run plot
- c. Box-Cox plot for power transforms

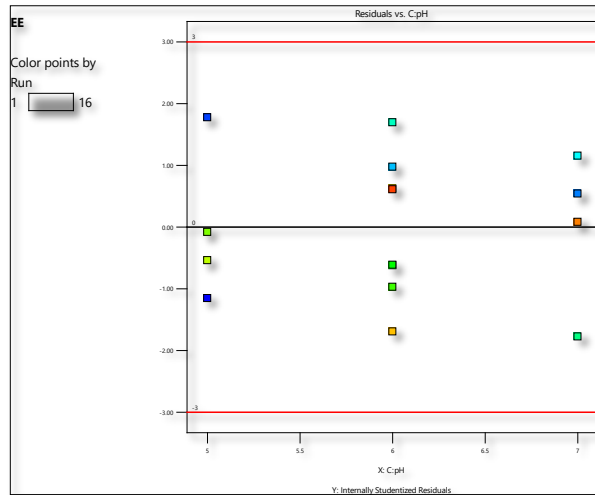
Various diagnostic plots for the evaluation of the model are shown in figure- 7.5. The **predicted Vs actual plot** (figure-7.5a) followed a 45° straight line, which indicated a close estimation of actual values with predicted values. The **residual versus run plot** (figure-7.5b) showed that the residuals were distributed randomly. This may indicate that there are no unidentified or hidden variables influencing the observed data. The **Box-Cox plot** (figure-7.5c) showed the best λ values (-0.03) was lie nearer to the current λ value of 1, indicating that there was no power transformation required.



a. Residuals Vs Chitosan concentration



b. Residuals Vs CS:CHON ratio



c. Residuals Vs pH of chitosan solution

Figure- 7.6. Residual Vs factor plots

- Residuals Vs Chitosan concentration
- Residuals Vs CS:CHON ratio
- Residuals Vs pH of chitosan solution

The plots for residuals with each factor (shown in figure- 7.6) represents a random scattering over the increasing levels of factor indicating that the model is effective in accounting for the variance for each factor.

Model Plots: Response surface plot (3D)

The ANOVA data indicate which variables have a significant influence on entrapment efficiency, as seen in the response surface 3D plot (shown in figure- 7.4d). The results showed that an increase in the concentration of chitosan increases the % EE, which may be attributed to the relative increase in the amount of polymer, leading to more polymeric network spaces within nanoparticles for drug entrapment [3, 5]. A 3D surface plot (figure- 7.4d) and the positive magnitude of factor A (equation-7.6) showed that an increase in the concentration of chitosan increases the entrapment efficiency.

From the 3D surface plot (figure-7.4e) and polynomial equation (equation-7.6), it was revealed that the decrease in entrapment efficiency with the increase in CS:CHON ratio was attributed to the drug leached from the polyelectrolyte complex nanoparticles due to insufficient or loose crosslinking between the oppositely charged

polyelectrolytes. This decreased EE may be due to the fact that CHON remains constant as chitosan concentration increases and is unable to interact with all available positively charged chitosan [3, 6].

The entrapment efficiency decreased with an increase in pH of the chitosan solution (figure-7.4f) because at pH 5, chitosan is easily and tightly crosslinked with the CHON and more drug can be entrapped within nanoparticles. As the pH of chitosan solution increases, the density of NH_3^+ decreases as it interacts with negatively charged CHON, which leads to the formation of loosely aggregated nanoparticles and results in the leaching of drug from nanoparticles [7].

The polynomial equations were obtained from design for entrapment efficiency are as follows:

$$\begin{aligned} \text{Entrapment Efficiency (\%)} = & + 62.52 + 9.66 * A - 2.52 * B - 7.15 * C + 2.09 * \\ & AB - 1.38 * AC - 0.7075 * BC - 8.65 * A^2 + 5.33 \\ & * B^2 + 1.74 * C^2 \\ & \dots\dots\dots \text{equation- 7.6} \end{aligned}$$

Reduced equation in terms of coded factors:

$$\begin{aligned} \text{Entrapment Efficiency (\%)} = & + 62.52 + 9.66 * A - 2.52 * B - 7.15 * C - 8.65 \\ & * A^2 + 5.33 * B^2 \\ & \dots\dots\dots \text{equation- 7.7} \end{aligned}$$

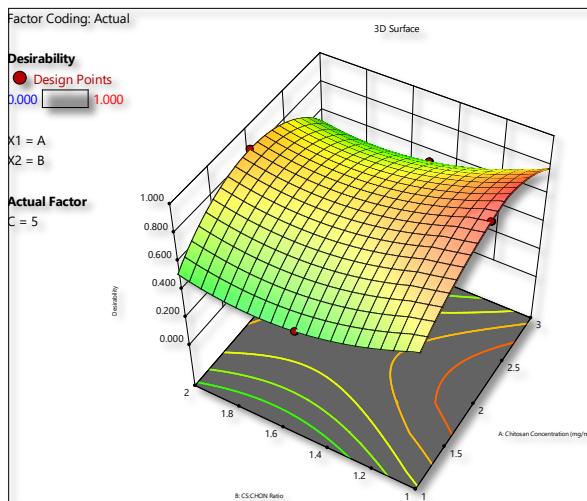
7.15. Desirability plot and overlay plot for optimization:

A desirability plot suggests the optimal values for each variable to get the desired results. DesignExpert 13.0.0 was used to generate this plot, and the table-7.14 below represents the desirable batch parameters.

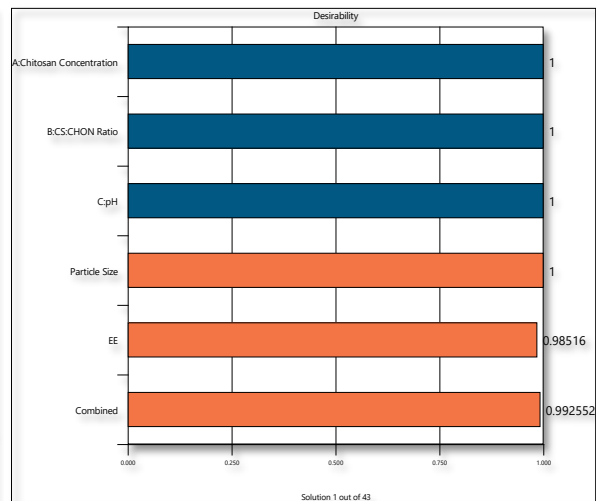
Table- 7.14. Variables for desirability plot and goals for response

| Name | Goal | Lower Limit | Upper Limit |
|--|-------------|-------------|-------------|
| A: Chitosan Concentration (mg/mL) | Is in range | 1 | 3 |
| B: CS:CHON Ratio | Is in range | 1:1 | 2:1 |
| C: pH of chitosan solution | Is in range | 5 | 7 |
| Particle Size (d.nm) | Minimize | 214.3 | 484.6 |
| EE (%) | Maximize | 40.29 | 80.79 |

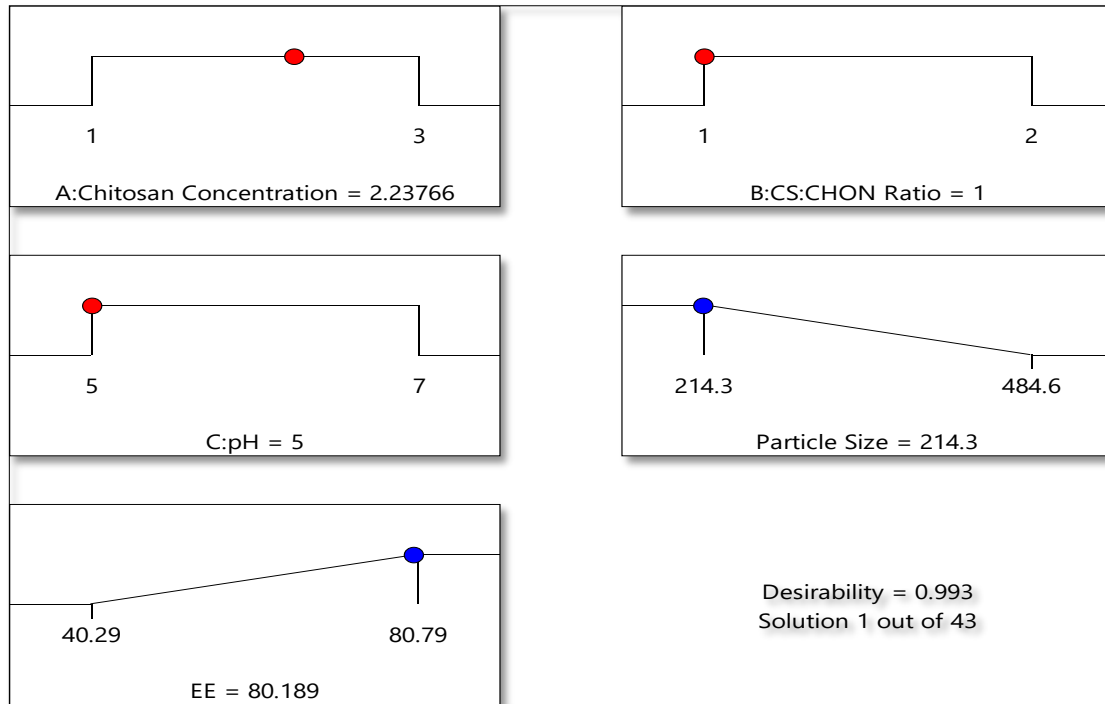
Desirability criteria and a desirability plot were developed in order to carry out optimization using mathematical function. For this, higher and lower desired response values were chosen, and software created variable values to help produce the desired response. The ramp graph (figure-7.7c) shows the projected values of R1 and R2 for the optimal concentration of independent variables, while the bar graph (figure-7.7b) shows individual desire for R1 and R2. The projected answer has a composite desirability of 0.993 (shown in figure- 7.7).



a. 3D Desirability plot



b. Desirability plot



c. Desirability plot

Figure- 7.7. Desirability plots for ATO loaded PECN

- 3D desirability plot
- Plot showing desirability value of all variables
- Desirability plot showing check point batch values

To evaluate the desirability, ATO loaded PECN formulation was prepared according to the suggested batch, and the obtained response values were determined to be similar with the predicted responses. Furthermore, the design's error was determined to be less than 5%, indicating its eligibility for prediction. This demonstrates that the software-predicted optimum formulation is reliable for practical purposes.

7.16. Assessment of the optimized ATO loaded PECN:

Based on the criteria of maximum entrapment efficiency and minimum particle size, the optimized batch of ATO-loaded PECN was obtained from the design space plot. As a result, a new batch of PECN was prepared to confirm the reliability of optimization design. The suggested optimized nanoparticles composition was used for the preparation of nanoparticles. The observed data was found to be aligned with the predicted values (shown in table- 7.15). The minimum % error was found in between observed values and

predicted values showing the Box-Behnken design's reliability and efficiency with no significant difference ($p < 0.05$). Thus, the results of the study showed that the ATO-loaded PECNs developed using BBD had the desired physicochemical characteristics.

Table- 7.15. Predicted and observed responses of optimized ATO loaded PECN

| Variables | Values | Responses | Predicted values | Observed values | % Error |
|---------------------------------------|--------|------------------|------------------|-----------------|---------|
| Chitosan concentration (mg/mL) | 2.24 | PS (d.nm) | 214.30 | 219.2 ± 5.98 | 2.24 |
| CS:CHON Ratio | 1:1 | EE (%) | 80.18 | 82.68 ± 2.63 | 3.22 |
| pH of Chitosan solution | 5.0 | | | | |

(n=3, ± S.D.)

7.17. Graphical optimization to generate control space:

The overlay plot of design is shown in figure- 7.8. The overlay plot is essential to select area that gives best values for both the dependent variables. This plot was generated by superimposing counter plots of both responses in factor space, which displaces the region of feasible response values. In figure-7.8, yellow region is the area where a little variation in the critical variables has no influence on the response and observed responses falls within the desired range. These approaches strengthen the design y narrowing design space and providing tolerance interval of alpha level of 0.05 to the responses.

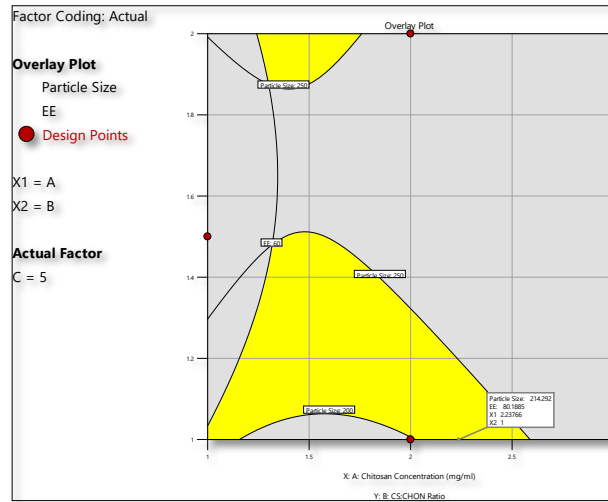


Figure- 7.8. Overlay plot for design space

7.18. Analysis of design space:

Three formulations were picked at random from the plotted design space to analyse the robustness of design space (shown in figure- 7.9). The formulation was generated using the provided values for the factors, and the predicted and observed values of the responses were compared.

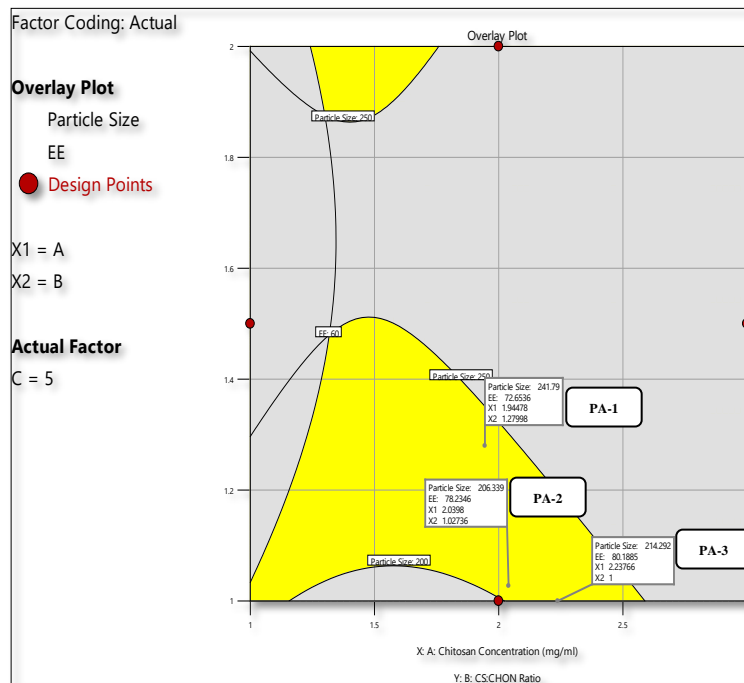


Figure- 7.9. Analysis of design space

Table- 7.16. Check point batch analysis

| Formulations | Parameters | Predicted | Observed | Std. Error |
|--------------|------------|-----------|--------------|------------|
| PA-1 | PS (d.nm) | 241.79 | 248.2 ± 9.33 | 2.65 |
| | % EE | 72.65 | 74.28 ± 1.27 | 2.24 |
| PA-2 | PS (d.nm) | 206.33 | 214.5 ± 7.28 | 3.95 |
| | % EE | 78.23 | 77.48 ± 2.61 | 0.96 |
| PA-3 | PS (d.nm) | 214.29 | 208.1 ± 5.36 | 2.88 |
| | % EE | 80.18 | 81.34 ± 1.98 | 1.44 |

(n=3, ± S.D.)

According to the robustness analysis (shown in table- 7.16), the observed responses remained within the boundary, and the variation between predicted and observed values was not significant.

7.19. Point prediction and confirmation:

The optimized values of responses were confirmed by carrying out the experiment using the selected factor values in triplicate. On the basis of results (shown in table- 7.17), it was confirmed that the observed and predicted values was found to be good agreement concluding the suitability of the selected model for optimization.

Table- 7.17. Predicted responses for selected solution along with standard deviation

| Analysis | Predicted Mean | Observed | Std Dev | n | SE Pred | 95% PI low | 95% PI high |
|-----------|----------------|--------------|---------|---|---------|------------|-------------|
| PS (d.nm) | 214.3 | 219.2 ± 5.98 | 17.33 | 3 | 18.22 | 169.71 | 258.88 |
| % EE | 80.1889 | 82.68 ± 2.63 | 2.52 | 3 | 2.65 | 73.70 | 86.67 |

(n=3, ± S.D.)

7.20. Physicochemical characteristics of ATO loaded PECN:

7.20.1. Particle size, % EE, % drug loading capacity and surface charge analysis:

The average particle size of optimized ATO loaded PECN was found to be 219.2 ± 5.98 d.nm with PDI of 0.218 ± 0.085 (shown in figure- 7.10). Nanoparticles with a PDI of less than 0.3 generally indicate uniform monodispersity [10, 33]. The % EE was found to be 82.68 ± 2.63 % with % drug loading capacity of 6.67 ± 0.098 %. The surface charge of ATO loaded PECN was found to be 25.41 ± 3.29 mV (shown in figure- 7.11). Due to electrostatic repulsion of individual particles, nanoparticles with a high positive zeta potential imply good physical stability of nanoparticles [1, 11].

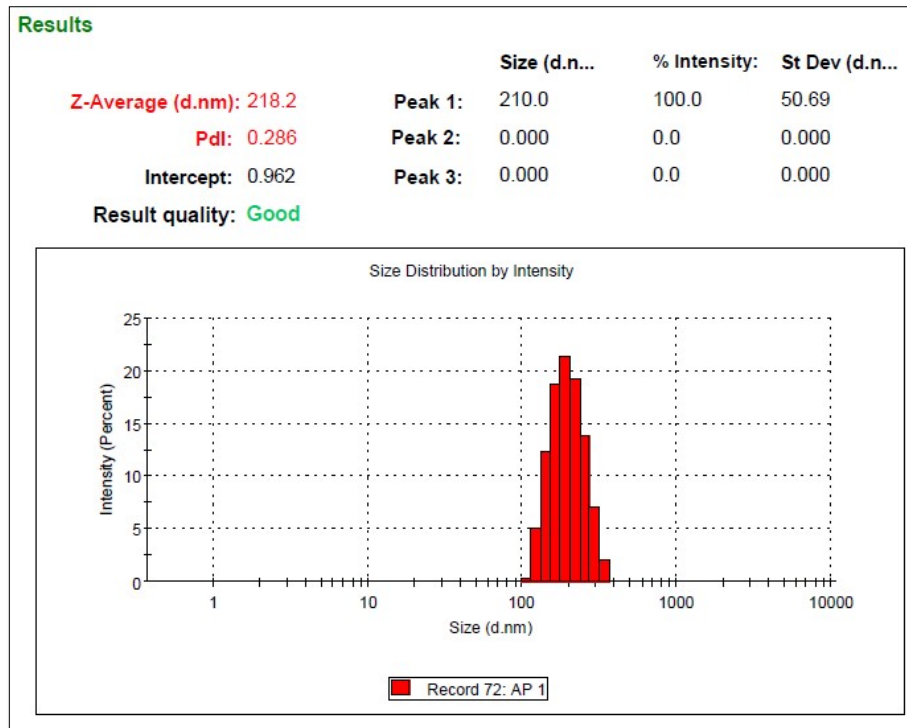


Figure- 7.10. Particle size analysis by zetasizer

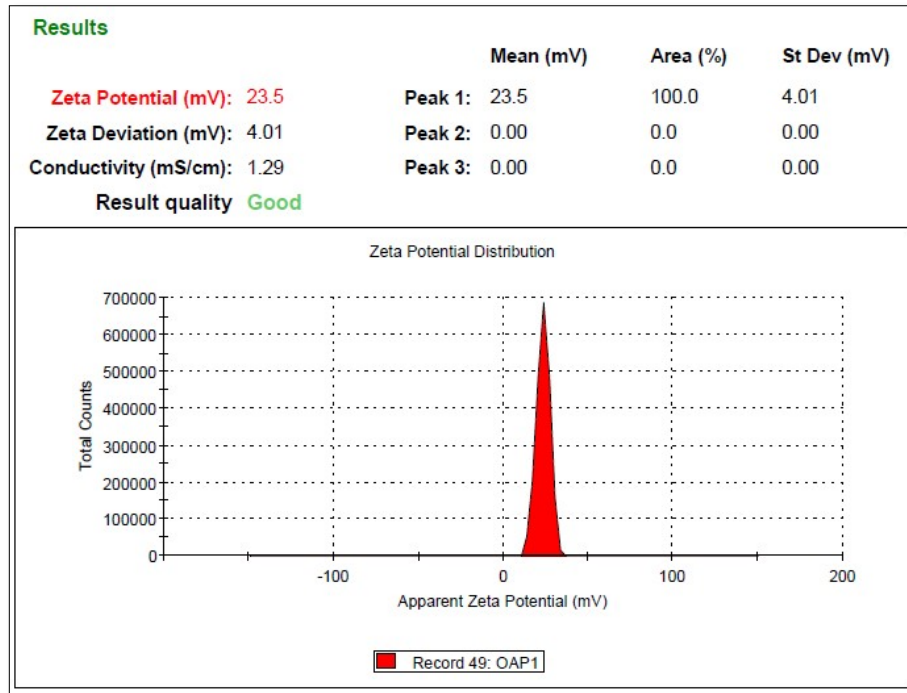


Figure- 7.11. Surface charge analysis by zetasizer

7.20.2. Surface morphological analysis:

TEM images of ATO loaded PECN revealed well-defined separated spherical shaped particles with homogeneous morphology with particle size less than 200 nm which was smaller than particle size of DLS analysis (shown in figure- 7.12). This happened due to the presence of a water layer on the surface of nanoparticles in dynamic light scattering method (by zetasizer), while the sample in the TEM analysis was in a dried state [34, 35].

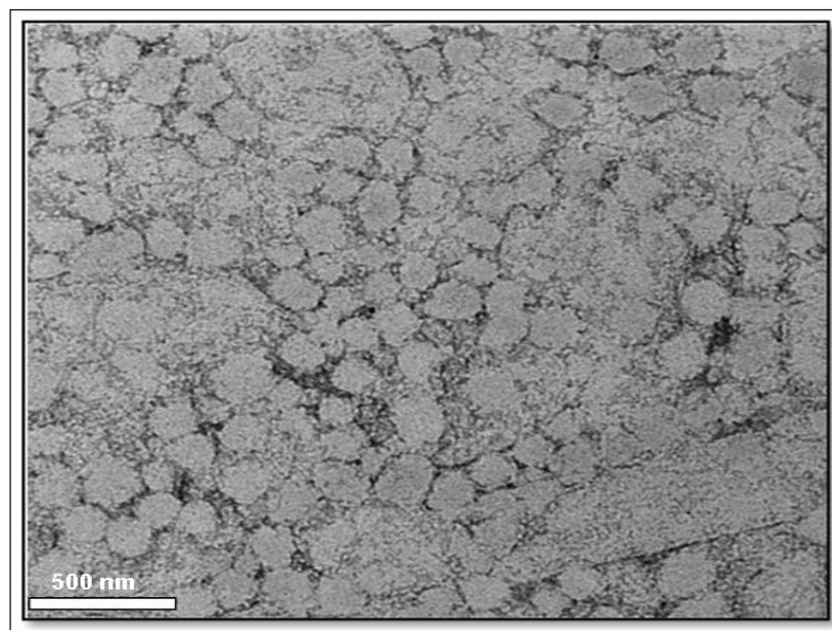
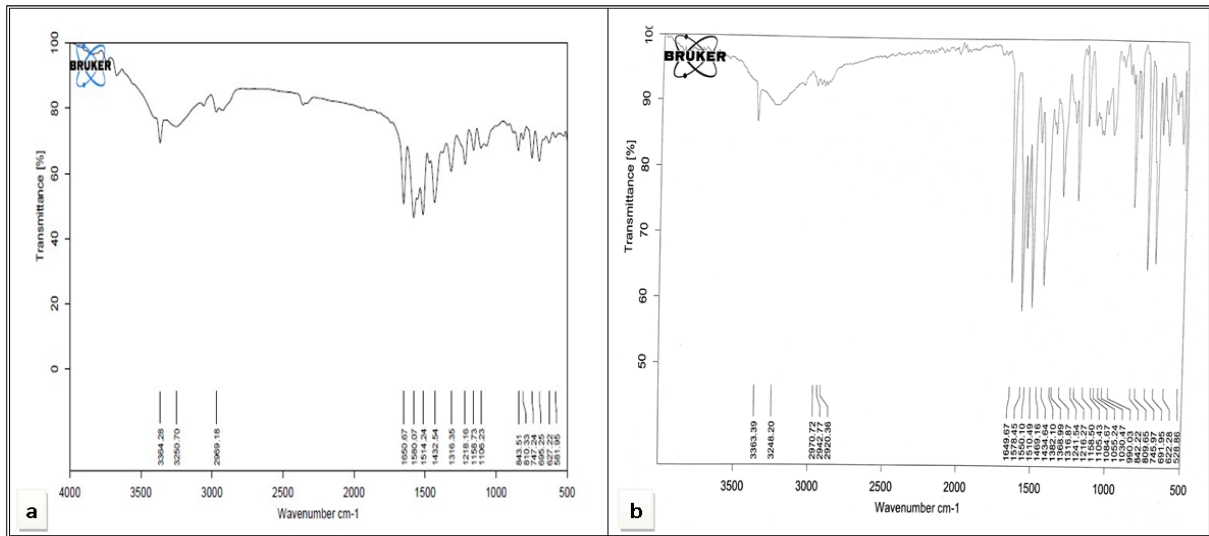


Figure- 7.12. TEM analysis of ATO loaded PECN

7.20.3. FTIR analysis:

The compatibility of ATO with excipients in the PEC nanoparticles was confirmed through their spectral analysis. The FTIR spectra of ATO and ATO loaded PECN are shown in figure- 7.13. The spectra of ATO represents broad band in domain of $3650-2850\text{ cm}^{-1}$, due to presence at 3363.85 cm^{-1} for -NH stretching and at 3055.24 cm^{-1} for -CH stretching. The other characteristic peaks found at 1656.85 cm^{-1} represent C=O stretching for amide carbonyl and 1683.86 cm^{-1} for carboxylate, 1317.38 cm^{-1} represent C-N stretching, 1523.76 cm^{-1} for N-H in plane bending (angular deformation) and 1215.15 cm^{-1} represent C-F stretching. All characteristic peaks of atorvastatin were retained with minor change in peak intensity in FTIR spectra of ATO loaded PECN. There were no interactions occurring between drug and excipients present in formulation suggesting that ATO maintained its structural integrity and compatibility with all excipients.



Figure– 7.13. FTIR spectra of atorvastatin (a) and atorvastatin loaded PECN (b)

7.20.4. DSC analysis:

Thermograms of pure drug (ATO) and ATO loaded PECN are shown in figure- 7.14. The melting point of ATO is represented by intensive endothermic peak at 166.19 °C which indicates the crystalline nature of ATO. The peak of ATO disappeared in thermogram of ATO loaded PECN indicating transformation of crystalline into molecular structures due to complete encapsulation of ATO in polymeric matrix [10].

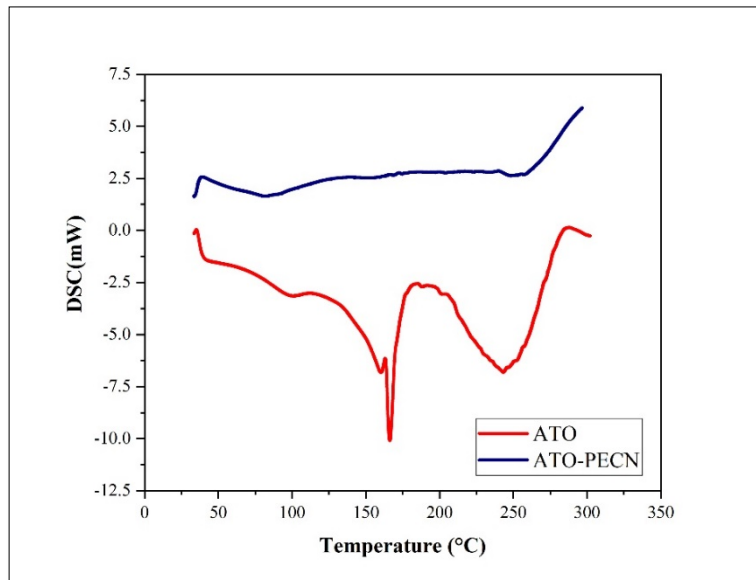


Figure- 7.14. DSC thermogram of ATO and ATO PECN

7.20.5. X-ray diffraction study:

XRD analysis of ATO and ATO loaded PECN are shown in figure- 7.15. The XRD diffractogram of ATO showed the presence of many sharp peaks which indicated its crystalline nature. The XRD profile of ATO-loaded PECN revealed the disappearance of intense ATO characteristic peaks, confirming drug encapsulation within polymeric matrix and indicating its amorphous state in the formulation.

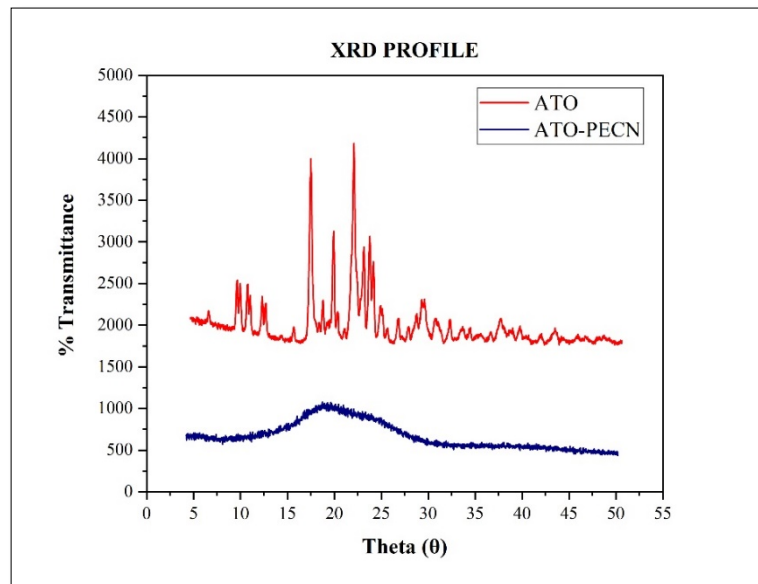


Figure- 7.15. X-ray Diffractogram of ATO and ATO-PECN

7.21. *In vitro* drug release study:

The optimized batch of ATO loaded PECN and pure drug were analyzed for cumulative drug release at physiological blood pH i.e. PBS 7.4 (table- 7.18) and skin pH i.e., PBS 5.5 (table- 7.19) using dialysis bag method (figure- 7.16). There was 99.66 ± 2.26 % and 98.85 ± 1.31 % of drug release from pure drug at pH PBS 7.4 and PBS 5.5 within 7 hrs and 8 hrs respectively. 62.96 ± 1.55 % and 99.61 ± 2.53 % of drug was release from ATO loaded PECN at pH 5.5 and 7.4 respectively within 48 hrs. The release of ATO was very slow at pH 5.5 as compared to PBS 7.4. The release pattern of PECN showed sustained release by diffusion of drug through polymer matrix. Drug release was relatively slow at pH 5.5 which might be due to the fact that at this pH, chitosan is easily and tightly crosslinked with CHON and forms stable PECN, which prevents the drug from being easily released from the nanoparticles [5].

The obtained data were fitted in various release models like Zero order, First order, Higuchi and Korsmeyer-Peppas model for both PBS 5.5 (figure- 7.17 and table- 7.20) as well as PBS 7.4 (figure- 7.18 and table- 7.21). The pure drug followed zero order kinetic with regression-coefficient of plot in pH 5.5 and pH 7.4 was found to be 0.9810 and 0.9790 respectively. ATO loaded PECN followed Higuchi model with regression-coefficient of 0.9762 and 0.9926 in PBS pH 5.5 and PBS pH 7.4 was found respectively, which was higher. The release exponent (n) values at PBS 5.5 and PBS 7.4 are shown in table- 7.20 and 7.21 respectively. It was observed that the pure drug (in pH 5.5 medium), ATO-PECN (in both medium) followed non-fickian or anomalous mechanism of release ($n = 0.45 < 0.85$); but in case of release from pure drug in pH 7.4 medium, it followed fickian mechanism of release ($n=0.45 < 0.85$) [36]. The erosion and diffusion were the major mechanism for drug release from nanoparticles. The sustained phase released the drug at a slower rate, which may have been owing to the diffusion of the entrapped drug inside the polymer's cross-linked matrix [5, 10, 35].

Table- 7.18. *In vitro* drug release profile for ATO loaded PECN in PBS 5.5

| Time (In Hrs) | Pure drug | ATO loaded PECN |
|---------------|--------------|-----------------|
| 0 | 0 ± 0 | 0 ± 0 |
| 0.5 | 19.31 ± 0.65 | 0.45 ± 0.18 |
| 1 | 30.20 ± 1.05 | 1.13 ± 0.61 |
| 1.5 | 38.21 ± 2.00 | 3.25 ± 0.98 |
| 2 | 46.58 ± 0.89 | 5.74 ± 1.21 |
| 3 | 58.02 ± 1.20 | 10.11 ± 1.23 |
| 4 | 70.32 ± 0.96 | 14.27 ± 1.56 |
| 5 | 78.52 ± 1.96 | 18.46 ± 2.53 |
| 6 | 91.98 ± 1.12 | 19.37 ± 2.74 |
| 8 | 99.66 ± 0.71 | 22.01 ± 3.18 |
| 12 | | 27.87 ± 2.14 |
| 24 | | 36.58 ± 1.47 |
| 36 | | 44.84 ± 2.35 |
| 48 | | 62.96 ± 4.56 |

(n=3, ±S.D.)

Table- 7.19. *In vitro* drug release profile of ATO loaded PECN in PBS 7.4

| Time (In Hrs) | Pure drug | ATO loaded PECN |
|---------------|--------------|-----------------|
| 0 | 0 ± 0 | 0 ± 0 |
| 0.5 | 21.96 ± 2.59 | 4.33 ± 1.15 |
| 1 | 30.24 ± 2.03 | 10.29 ± 2.41 |
| 1.5 | 36.76 ± 1.34 | 16.35 ± 3.64 |
| 2 | 42.72 ± 1.09 | 21.59 ± 1.24 |
| 3 | 51.82 ± 1.21 | 24.18 ± 1.57 |
| 4 | 61.48 ± 0.68 | 28.62 ± 2.52 |
| 5 | 70.65 ± 0.93 | 32.66 ± 2.87 |
| 6 | 82.74 ± 1.17 | 35.49 ± 1.47 |
| 8 | 98.85 ± 0.89 | 43.08 ± 2.96 |
| 10 | | 54.72 ± 4.55 |
| 12 | | 73.75 ± 3.41 |
| 24 | | 94.74 ± 2.69 |
| 48 | | 99.61 ± 2.64 |

(n=3, ±S.D.)

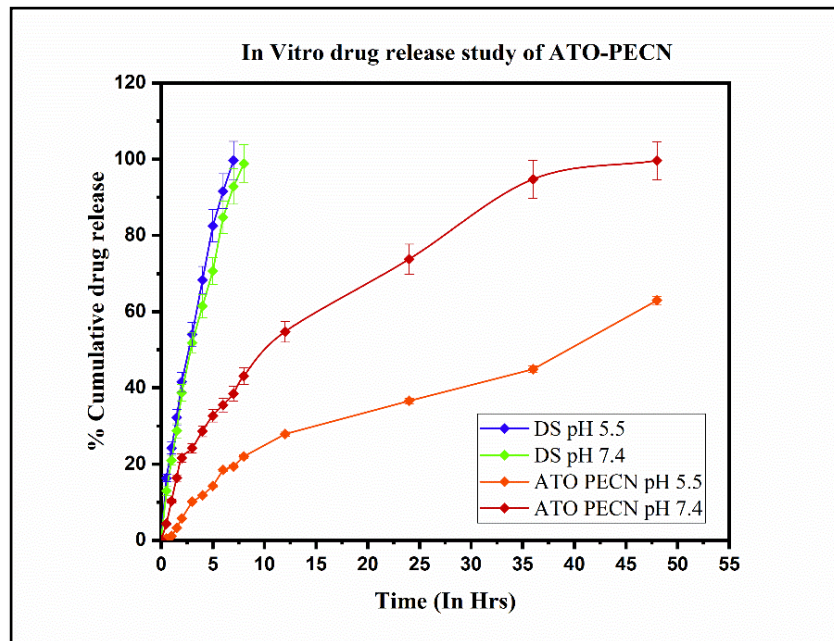
Figure- 7.16. *In vitro* cumulative drug release profile in PBS 5.5 and 7.4

Table- 7.20. Drug release kinetic models for ATO loaded PECN in pH 5.5

| Kinetic Models | Pure drug | ATO loaded PECN |
|--------------------------|----------------|-----------------|
| Zero order | 0.9810 | 0.9361 |
| First order | 0.7600 | 0.9630 |
| Higuchi | 0.9796 | 0.9762 |
| Korsemeyer-Peppas | 0.4989 | 0.9123 |
| (n) | (0.606) | (0.642) |

Table- 7.21. Drug release kinetic models for ATO loaded PECN in pH 7.4

| Kinetic Models | Pure drug | ATO loaded PECN |
|--------------------------|----------------|-----------------|
| Zero order | 0.9790 | 0.9012 |
| First order | 0.8511 | 0.9302 |
| Higuchi | 0.9758 | 0.9926 |
| Korsemeyer-Peppas | 0.5671 | 0.7479 |
| (n) | (0.381) | (0.518) |

7.22. *Ex vivo* skin permeation study:

The ex-vivo skin permeation of pure drug and ATO loaded PECN were performed using rat skin on Franz diffusion cell is shown in figure-7.17 and table- 7.22. The % amount of drug permeated through skin from pure drug after 48 hrs was 35.67 ± 1.73 %. In case of ATO loaded PECN, the % drug permeated through skin was found to be 55.23 ± 2.19 % in 48 hrs. The drug permeability through skin was enhanced 1.58 folds as compared to pure drug might be due to nanosize particles that permeated through skin layers. The presence of chitosan hydrates the stratum corneum and electrostatically interacts with skin proteins and it reversibly modifies keratin protein structure to create pathway for drug permeation [5, 37, 38]. Chitosan improved skin penetration through trans-appendageal and transcellular pathway [5]. The results of this study also confirmed the nanocarrier's ability to enhance skin permeability. The average flux of pure drug was found to be 0.76 ± 0.13 $\mu\text{g}/\text{cm}^2/\text{hr}$ and for ATO loaded PECN was found to be 1.58 ± 0.22 $\mu\text{g}/\text{cm}^2/\text{hr}$, which was 2.07 folds enhanced as compared to pure drug. The steady state flux for pure drug was found to be 0.73 ± 0.11 $\mu\text{g}/\text{cm}^2/\text{hr}$; the steady state flux for ATO-PECN was found to be 1.05 ± 0.25 $\mu\text{g}/\text{cm}^2/\text{hr}$ and was 1.51 folds enhanced as

compared to pure drug. These results clearly imply that ATO loaded PEC nanoparticles showed potential for transdermal drug delivery.

Table- 7.22. *Ex vivo* skin permeation profile

| Time (In hrs) | ATO loaded PECN | Pure drug |
|--|------------------------|------------------|
| 0 | 0 ± 0 | 0 ± 0 |
| 0.5 | 1.10 ± 0.34 | 0 ± 0 |
| 1 | 1.84 ± 0.78 | 0.40 ± 0 |
| 2 | 3.07 ± 1.02 | 1.18 ± 0.25 |
| 3 | 3.86 ± 1.54 | 1.87 ± 0.32 |
| 4 | 6.60 ± 1.21 | 3.55 ± 0.66 |
| 5 | 9.11 ± 0.88 | 4.87 ± 0.63 |
| 6 | 12.65 ± 1.26 | 5.05 ± 0.94 |
| 7 | 14.25 ± 1.54 | 7.12 ± 0.67 |
| 8 | 18.29 ± 2.15 | 9.76 ± 0.98 |
| 10 | 22.06 ± 1.09 | 11.78 ± 1.19 |
| 12 | 24.41 ± 1.04 | 14.39 ± 1.05 |
| 24 | 35.71 ± 2.33 | 23.89 ± 0.71 |
| 36 | 48.51 ± 2.48 | 29.13 ± 0.71 |
| 48 | 55.23 ± 2.19 | 35.67 ± 1.73 |
| Parameters | ATO loaded PECN | Pure drug |
| Drug remain on skin (%) | 19.12 ± 3.04 | 52.07 ± 4.54 |
| Drug retain in skin (%) | 26.86 ± 2.21 | 10.39 ± 1.95 |
| Transdermal flux (% drug permeated/cm²/hr) | 1.58 | 0.76 |
| Steady state flux | 1.04 | 0.69 |

PER (as compared to
pure ATO)

2.07

1

(n=3, \pm S.D.)

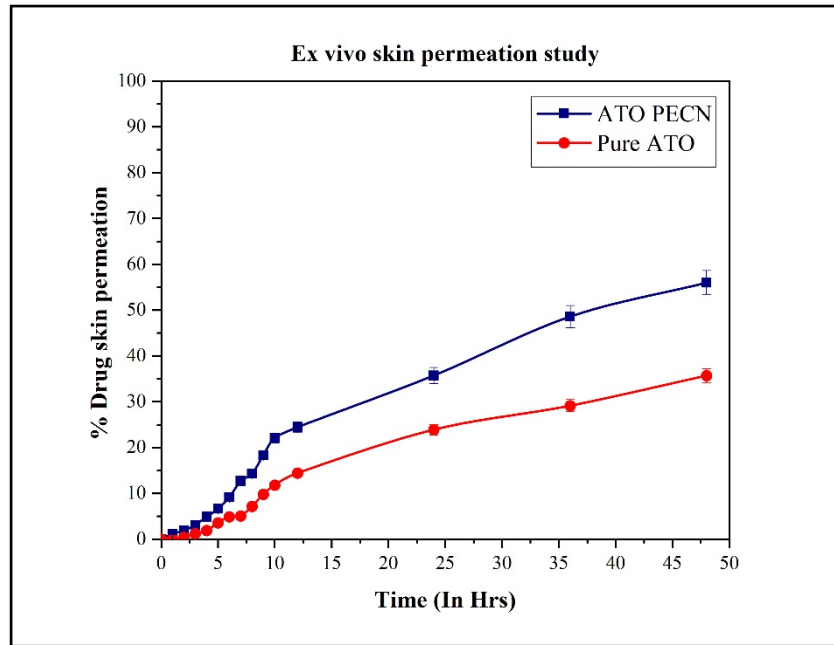


Figure-7.17. *Ex vivo* skin permeation study profile

7.23. *In vitro* cell viability study:

The study was assessed by MTT assay to check the cell viability of formulation. On the basis of results, it was concluded that there were no significant effects observed in cell viability of placebo PECN and ATO loaded PECN after 12 hrs (figure- 7.18a) and 24 hrs (figure- 7.18b). The ATO loaded PECN and placebo PECN showed cell viability greater than 95% in 24 hrs and showed better viability than pure drug (90% cell viability in 24 hrs). On the basis of results, it was concluded that the PECN showed no toxicity to fibroblast cells and was safe to use in transdermal drug delivery systems.

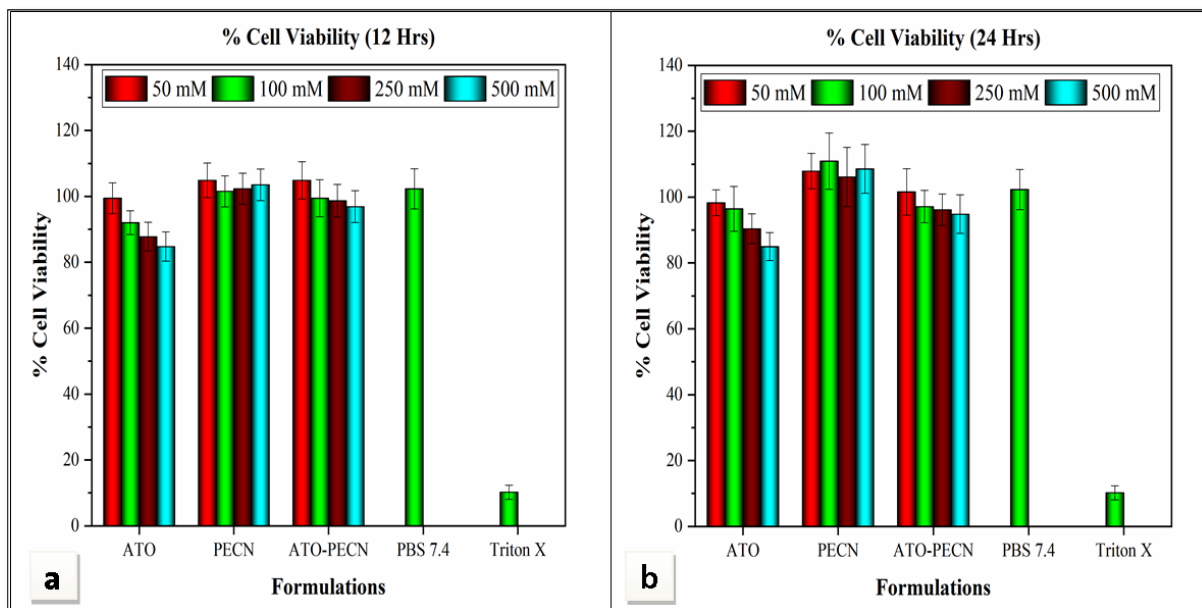


Figure- 7.18. % Cell viability study for 12 hrs (a) and 24 Hrs (b)

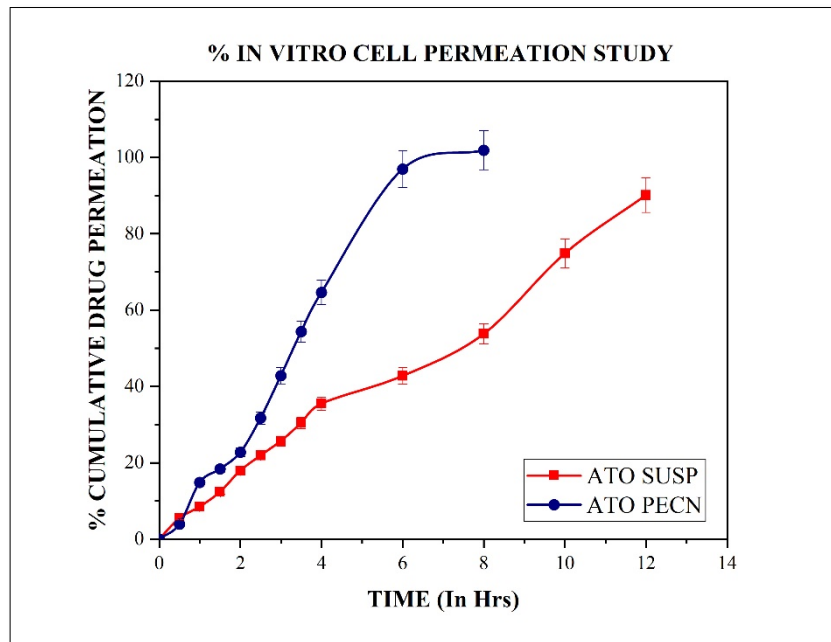
7.24. *In vitro* cell permeability study:

The rate limiting barrier of skin is stratum corneum layer for transdermal drug delivery. The cell monolayer integrity was monitored by TEER values for 21-25 days and this value should be in the range of 500 to 1000 Ωcm^2 for acceptable transport mechanism [20-22]. Apparent permeability coefficient (P_{app}) greater than 1×10^{-5} cm/s is considered as highly permeable substance [39, 40]. The TEER value of cell permeability at 21 days was found to be 920 Ωcm^2 and it represented a good quality of development of cell layers [20-22]. The ATO loaded PECN showed P_{app} value of 1.05×10^{-5} cm/s, while pure drug showed value of 6.17×10^{-6} cm/s. The % amount of drug permeated through cell per unit time is shown in figure- 7.19 and table- 7.23. The results revealed that in the case of pure drug, approximately 90% of the drug permeated the cell within 12 hours, whereas ATO PECN permeated 90% of the drug through the cells within 6–8 hours. The higher permeation of ATO from ATO-PECN due to interaction of positively charged PECN with the negatively charged sites on cell surface and opens the intracellular tight junctions which accompanies the paracellular permeability [41]. On the basis of results, it was concluded that the PECN showed more cell permeability as compared to pure drug, due to nanosize of formulation and highly positive surface charge which facilitated permeation of drug through cell layers.

Table- 7.23. *In vitro* cell permeability profile

| Time (In Hrs) | Pure drug | ATO-PECN |
|------------------|-----------------------|-----------------------|
| 0 | 0 ± 0 | 0 ± 0 |
| 1 | 8.5 ± 1.4 | 14.83 ± 2.09 |
| 2 | 17.94 ± 1.89 | 22.74 ± 1.13 |
| 3 | 25.71 ± 1.28 | 42.83 ± 2.14 |
| 4 | 35.49 ± 1.77 | 64.61 ± 3.23 |
| 6 | 42.76 ± 2.13 | 96.96 ± 4.84 |
| 8 | 53.74 ± 2.68 | |
| 10 | 74.84 ± 3.74 | |
| 12 | 90.12 ± 4.56 | |
| P_{app} (cm/s) | 6.17×10^{-6} | 1.05×10^{-5} |

(n=3, ±S.D.)

Figure- 7.19. *In vitro* cell permeability profile

7.25. Stability study:

The physicochemical parameters like particle size and % assay affected by different storage conditions, viz. 2-8 °C, 25±2°C/60 ± 5 % RH and 40±2°C/75 ± 5 % RH are shown in figure- 7.20 and table- 7.24. The results showed that no significant change was observed in particle size and % assay in PECN at 2-8 °C and 25±2°C/60 ± 5 % RH over 90 days. There was significant increase in particle size with reduction in % assay at 40±2°C/75 ± 5 % RH over 90 days due to agglomeration of particles and drug leakage from nanoparticles [42]. Based on results, it was concluded that the ATO loaded PECNs were stable at 2-8 °C and 25±2°C/60 ± 5 % RH.

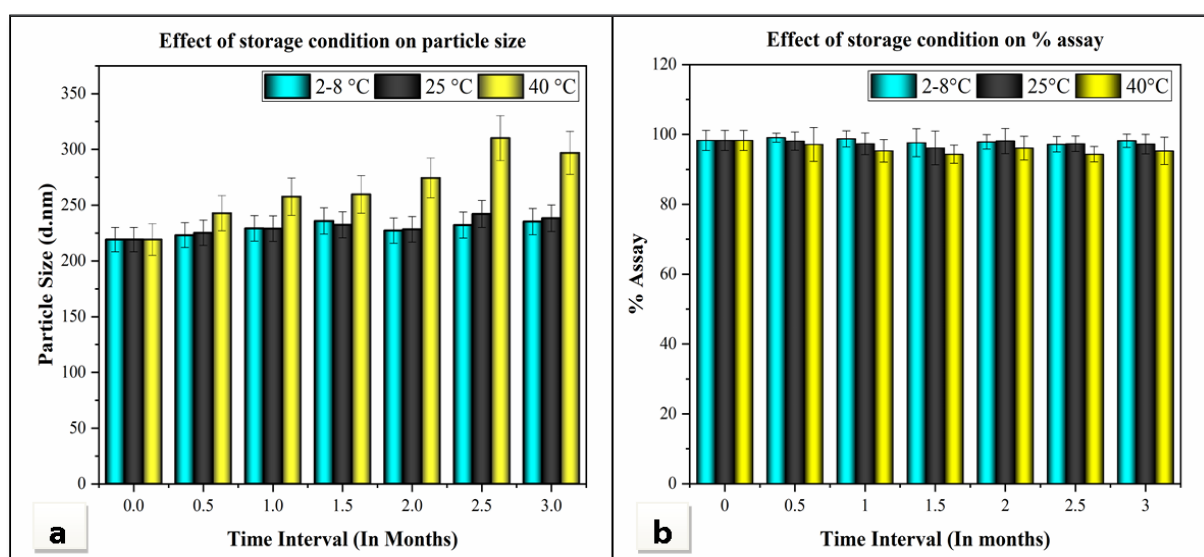


Figure- 7.20. Effect of storage condition on particle size (a) and % assay (b).

Table- 7.24. Stability study profile

| Sr. No. | Time interval (In Month) | Particle Size (d.nm) | | | % Assay | | |
|---------|-----------------------------|----------------------|-----------------------|-----------------------|--------------|-----------------------|-----------------------|
| | | 2-8°C | 25±2°C/60 ± 5 % RH | 40±2°C/75 ± 5 % RH | 2-8°C | 25±2°C/60 ± 5 % RH | 40±2°C/75 ± 5 % RH |
| 1 | Initial | 219.2 ± 5.98 | 219.2 ± 5.98 | 219.2 ± 5.98 | 98.30 ± 1.28 | 98.30 ± 1.28 | 98.30 ± 1.28 |
| 2 | 0.5 | 223.1 ± 6.24 | 225.3 ± 4.45 | 242.9 ± 3.29 | 99.01 ± 2.51 | 98.23 ± 2.21 | 97.16 ± 1.08 |
| 3 | 1.0 | 229.2 ± 4.63 | 229.1 ± 4.51 | 257.7 ± 4.74 | 98.75 ± 2.26 | 97.36 ± 3.39 | 95.32 ± 2.96 |
| 4 | 1.5 | 235.9 ± 4.19 | 232.4 ± 6.51 | 259.7 ± 5.67 | 97.63 ± 3.21 | 96.15 ± 1.10 | 94.36 ± 2.41 |
| 5 | 2.0 | 227.3 ± 5.39 | 228.4 ± 4.92 | 274.5 ± 5.24 | 97.89 ± 2.45 | 98.15 ± 1.63 | 96.11 ± 2.66 |
| 6 | 2.5 | 232.2 ± 5.47 | 242.1 ± 3.47 | 310.2 ± 6.88 | 97.21 ± 2.46 | 97.36 ± 1.86 | 94.64 ± 1.14 |
| 7 | 3.0 | 235.3 ± 4.81 | 238.3 ± 5.21 | 296.9 ± 10.36 | 98.25 ± 2.09 | 97.60 ± 2.54 | 95.30 ± 1.09 |

(n=3, ±S.D.)

Chapter 7 – ATO loaded PECN**7.26. References:**

1. Joseph, E., G.J.N.f.d.d. Singhvi, and therapy, *Multifunctional nanocrystals for cancer therapy: a potential nanocarrier*. Nanomaterials for Drug Delivery and Therapy, 2019: p. 91-116.
2. Liang, T., Z. Zhang, and P.J.F.c. Jing, *Black rice anthocyanins embedded in self-assembled chitosan/chondroitin sulfate nanoparticles enhance apoptosis in HCT-116 cells*. Food Chemistry, 2019. **301**: p. 125280.
3. Kumar, A. and M.J.I.j.o.b.m. Ahuja, *Carboxymethyl gum kondagogu–chitosan polyelectrolyte complex nanoparticles: Preparation and characterization*. International Journal of Biological Macromolecules, 2013. **62**: p. 80-84.
4. Umerska, A., O.I. Corrigan, and L.J.C.p. Tajber, *Design of chondroitin sulfate-based polyelectrolyte nanoplexes: Formation of nanocarriers with chitosan and a case study of salmon calcitonin*. Carbohydrate Polymers, 2017. **156**: p. 276-284.
5. Gul, R., et al., *Biodegradable ingredient-based emulgel loaded with ketoprofen nanoparticles*. AAPS PharmSciTech, 2018. **19**: p. 1869-1881.
6. Jardim, K.V., et al., *Physico-chemical characterization and cytotoxicity evaluation of curcumin loaded in chitosan/chondroitin sulfate nanoparticles*. Materials science and engineering: c, 2015. **56**: p. 294-304.
7. Rezazadeh, M., et al., *Incorporation of rosuvastatin-loaded chitosan/chondroitin sulfate nanoparticles into a thermosensitive hydrogel for bone tissue engineering: preparation, characterization, and cellular behavior*. Pharmaceutical Development and Technology, 2019. **24**(3): p. 357-367.
8. Kamani, P., et al., *Phospholipid based ultra-deformable nanovesicular gel for transcutaneous application: QbD based optimization, characterization and pharmacodynamic profiling*. Journal of Drug Delivery Science and Technology, 2019. **51**: p. 152-163.
9. Soe, Z.C., et al., *Folate-targeted nanostructured chitosan/chondroitin sulfate complex carriers for enhanced delivery of bortezomib to colorectal cancer cells*. Asian journal of pharmaceutical sciences, 2019. **14**(1): p. 40-51.

10. Faris, T.M., et al., *Developed simvastatin chitosan nanoparticles co-crosslinked with tripolyphosphate and chondroitin sulfate for ASGPR-mediated targeted HCC delivery with enhanced oral bioavailability*. Saudi Pharmaceutical Journal, 2020. **28**(12): p. 1851-1867.
11. Talib, S., et al., *Chitosan-chondroitin based artemether loaded nanoparticles for transdermal drug delivery system*. Journal of Drug Delivery Science and Technology, 2021. **61**: p. 102281.
12. Abdullah, T.A., N.J. Ibrahim, and M.H. Warsi, *Chondroitin sulfate-chitosan nanoparticles for ocular delivery of bromfenac sodium: Improved permeation, retention, and penetration*. International journal of pharmaceutical investigation, 2016. **6**(2): p. 96.
13. Mahmoud, M.O., et al., *Transdermal delivery of atorvastatin calcium from novel nanovesicular systems using polyethylene glycol fatty acid esters: ameliorated effect without liver toxicity in poloxamer 407-induced hyperlipidemic rats*. Journal of Controlled Release, 2017. **254**: p. 10-22.
14. Aboud, H.M., et al., *Development, optimization, and evaluation of carvedilol-loaded solid lipid nanoparticles for intranasal drug delivery*. AAPS pharmscitech, 2016. **17**(6): p. 1353-1365.
15. Segeritz, C.-P. and L. Vallier, *Cell culture: Growing cells as model systems in vitro*, in *Basic science methods for clinical researchers*. 2017, Elsevier. p. 151-172.
16. Helgason, C.D. and C.L. Miller, *Basic cell culture protocols*. 2005: Totowa, NJ.: Humana Press.
17. Tripathi, B.D. and N. Singh, *Wound Healing Potential of Transdermal Patches Containing Bioactive Fraction: A Novel Approach*. International Journal of Pharmacy & Life Sciences, 2020. **11**(7): p. 83-83.
18. Manca, M.L., et al., *Glycosomes: Use of hydrogenated soy phosphatidylcholine mixture and its effect on vesicle features and diclofenac skin penetration*. International Journal of Pharmaceutics, 2016. **511**(1): p. 198-204.
19. Manca, M.L., et al., *Glycosomes: A new tool for effective dermal and transdermal drug delivery*. International Journal of Pharmaceutics, 2013. **455**(1-2): p. 66-74.

20. Shah, P., et al., *In vitro assessment of acyclovir permeation across cell monolayers in the presence of absorption enhancers*. Drug development and industrial pharmacy, 2008. **34**(3): p. 279-288.
21. Chen, S., R. Einspanier, and J. Schoen, *Trans epithelial electrical resistance (TEER): a functional parameter to monitor the quality of oviduct epithelial cells cultured on filter supports*. Histochemistry and cell biology, 2015. **144**(5): p. 509-515.
22. Poenar, D.P., et al., *Low-cost method and biochip for measuring the trans-epithelial electrical resistance (TEER) of esophageal epithelium*. Materials, 2020. **13**(10): p. 2354.
23. Sharma, D., et al., *Formulation and optimization of polymeric nanoparticles for intranasal delivery of lorazepam using Box-Behnken design: in vitro and in vivo evaluation*. BioMed research international, 2014. **2014**.
24. Makoni, P.A., K. Wa Kasongo, and R.B. Walker, *Short term stability testing of efavirenz-loaded solid lipid nanoparticle (SLN) and nanostructured lipid carrier (NLC) dispersions*. Pharmaceutics, 2019. **11**(8): p. 397.
25. Al-Nemrawi, N., S. Alsharif, and R.J.I.J.A.P. Dave, *Preparation of chitosan-TPP nanoparticles: the influence of chitosan polymeric properties and formulation variables*. International Journal of Applied Pharmaceutics, 2018. **10**: p. 60-65.
26. Thandapani, G., et al., *Size optimization and in vitro biocompatibility studies of chitosan nanoparticles*. International Journal of Biological Macromolecules, 2017. **104**: p. 1794-1806.
27. Hussain, Z., S.J.I.J.o.P. Sahudin, and P. Sciences, *Preparation, characterisation and colloidal stability of chitosan-tripolyphosphate nanoparticles: optimisation of formulation and process parameters*. International Journal of Pharmacy and Pharmaceutical Sciences 2016. **8**(3): p. 297-308.
28. Sreeharsha, N., et al., *Development of metronidazole loaded chitosan nanoparticles using QbD approach—A novel and potential antibacterial formulation*. Pharmaceutics, 2020. **12**(10): p. 920.

29. Chuah, L.H., et al., *Curcumin-containing chitosan nanoparticles as a potential mucoadhesive delivery system to the colon*. Pharm Dev Technol. 2013. **18**(3): p. 591-599.
30. Hamman, J.H.J.M.d., *Chitosan based polyelectrolyte complexes as potential carrier materials in drug delivery systems*. Marine drugs, 2010. **8**(4): p. 1305-1322.
31. Sangshetti, J.N., et al., *Quality by design approach: Regulatory need*. Arabian Journal of Chemistry, 2017. **10**: p. S3412-S3425.
32. Vining, G.J.Q.E., *Technical advice: residual plots to check assumptions*. Quality Engineering, 2010. **23**(1): p. 105-110.
33. Abdullah, T.A., N.J. Ibrahim, and M.H.J.I.j.o.p.i. Warsi, *Chondroitin sulfate-chitosan nanoparticles for ocular delivery of bromfenac sodium: Improved permeation, retention, and penetration*. 2016. **6**(2): p. 96.
34. Onugwu, A.L., et al., *Development and optimization of solid lipid nanoparticles coated with chitosan and poly (2-ethyl-2-oxazoline) for ocular drug delivery of ciprofloxacin*. 2022. **74**: p. 103527.
35. Gul, R., et al., *Biodegradable ingredient-based emulgel loaded with ketoprofen nanoparticles*. 2018. **19**(4): p. 1869-1881.
36. Bruschi, M.L., *Strategies to modify the drug release from pharmaceutical systems*. 2015: Woodhead Publishing.
37. He, W., et al., *Study on the mechanisms of chitosan and its derivatives used as transdermal penetration enhancers*. international journal of pharmaceutics, 2009. **382**(1-2): p. 234-243.
38. Gul, R., et al., *Functionalised nanostructures for transdermal delivery of drug cargos*. Journal of drug targeting, 2018. **26**(2): p. 110-122.
39. Neupane, R., et al., *Alternatives to biological skin in permeation studies: Current trends and possibilities*. Pharmaceutics, 2020. **12**(2): p. 152.
40. Alvarez-Figueroa, M.J., et al., *Evaluation of the membrane permeability (PAMPA and skin) of benzimidazoles with potential cannabinoid activity and their relation with the*

Biopharmaceutics Classification System (BCS). AAPS PharmSciTech., 2011. **12**: p. 573-578.

41. Lin, Y.-H., et al., *Preparation of nanoparticles composed of chitosan/poly- γ -glutamic acid and evaluation of their permeability through Caco-2 cells*. *Biomacromolecules*, 2005. **6**(2): p. 1104-1112.
42. Malviya, R., et al., *Evaluation of Antitumor Efficacy of Chitosan-Tamarind Gum Polysaccharide Polyelectrolyte Complex Stabilized Nanoparticles of Simvastatin*. *Int J Nanomedicine*, 2021. **16**: p. 2533-2553.